

Diplomarbeit

Investigations on the influence of joint orientations for foundations on rock

ausgeführt zum Zwecke der Erlangung des akademischen Grads
Diplom-Ingenieur / Diplom-Ingenieurin
eingereicht an der TU Wien, Fakultät für Bau- und Umweltingenieurwesen

Diploma Thesis

Untersuchungen zum Einfluss der Trennflächenorientierungen bei Gründungen auf Fels

Submitted in satisfaction of the requirements for the degree of
Diplom-Ingenieur / Diplom-Ingenieurin
of the TU Wien, Faculty of Civil and Environmental Engineering

von

Hossein Rast Koutash

Matr.Nr.: 01428887

Betreuung: Privatdoz. Dipl.-Ing. Dr.techn. **Alexander Preh**
Institut für Geotechnik
Forschungsbereich Ingenieurgeologie
Technische Universität Wien,
Karlsplatz 13/220-A, 1040 Wien, Österreich

Wien, im März 2024

Abstract:

The present study aimed to investigate the influence of the orientation of joint set in foundations on fractured rock. A predefined failure mechanism, such as the sliding of a wedge on an interface, was analyzed in detail according to the ÖNORMEN B 1997-1-2 standards. Particular attention was given to considering the spatial orientation of interfaces in foundations through three-dimensional calculations.

The calculations were conducted using the following methods:

- The analytical limit equilibrium method by Ladanyi and Roy (1971).
- The computational program 3DEC, which allows for a numerical investigation based on the Discrete Element Method (DEM).

All investigations were carried out following the Mohr-Coulomb failure criterion. The strength parameters, namely cohesion and friction angle of potentially existing interfaces, were reduced compared to intact rock.

The comparison of calculation results using the above-mentioned methods clarifies that bearing capacity and failure mechanisms are significantly influenced by the mechanical properties, as well as the orientation and spacing of the joint set. However, since these variables were not adequately considered in the analytical contexts and ÖNORM standards, comparable results can only be obtained under specific conditions.

Considering the substantial differences in calculation results, the question arises as to whether the methods for assessing the load-bearing capacity of foundations on rock should be more precisely regulated in the relevant standards.

Kurzfassung:

Die vorliegende Studie hatte zum Ziel, den Einfluss der Ausrichtung von Trennflächen bei Gründungen auf geklüftetem Fels zu untersuchen. Dabei wurde ein vordefinierter Versagensmechanismus, wie beispielsweise das Gleiten eines Keilkörpers auf einer Trennfläche, gemäß den ÖNORMEN B 1997-1-2 detailliert analysiert.

Ein Besonderes Augenmerk lag hierbei auf der Berücksichtigung der räumlichen Orientierung der Trennflächen bei Gründungen mittels dreidimensionaler Berechnungen. Die Berechnungen wurden unter folgender Verwendung durchgeführt:

- des analytischen Grenzgleichgewichtsverfahren von Ladanyi and Roy (1971) .
- des Rechenprogramms 3DEC, das eine numerische Untersuchung auf Basis der Methode Diskrete-Elemente-Methode (DEM) ermöglicht

Alle Untersuchungen wurden nach dem Bruchkriterium von Mohr-Coulomb durchgeführt. Die Festigkeitsparameter, in diesem Fall Kohäsion und Reibungswinkel von möglicherweise vorhandenen Trennflächen, wurden im Vergleich zu ungeklüftetem Gestein reduziert. Der Vergleich der Berechnungsergebnisse mit den genannten Methoden verdeutlicht, dass die Tragfähigkeit und der Versagensmechanismus stark von den mechanischen Eigenschaften sowie der Ausrichtung und dem Abstand der Trennflächen zueinander abhängen. Da jedoch all diese Variablen in den analytischen Zusammenhängen und ÖNORMEN nicht hinreichend berücksichtigt wurden, ergeben sich vergleichbare Ergebnisse nur unter bestimmten Voraussetzungen.

Angesichts so großer Unterschiede der Berechnungsergebnisse stellt sich die Frage, ob in den einschlägigen Normen die Rechenverfahren zur Beurteilung der Tragfähigkeit von Gründungen auf Fels genauer geregelt werden sollten.

Acknowledgments:

Firstly, I would like to express my gratitude to my parents, Ali and Mehri, and my wife, Elham, who supported me during my studies and also in the time before, and throughout my education. Without them, this academic journey would not have been possible for me.

I want to express profound thanks to the research area of "Geotechnics."

Dr. Alexander Preh deserves special appreciation for not only providing significant support in shaping this work but also for his invaluable guidance. Additionally, the institute's generous provision of the necessary calculation programs (3DEC) has been crucial.

Furthermore, I would like to thank my fellow students with whom I have spent a significant amount of time both on and off the university campus in the past year.

Table of contents:

1 Introduction	10
1.1 Methods of assessing the bearing capacity of the foundation on rock	10
1.1.1 Experimental Method.....	11
1.1.2 Analytical Method	12
1.1.3 Numerical Method	12
1.1.3.1 Discontinuity Modeling Techniques	13
1.1.3.2 Continuous Modeling Techniques	13
2 Bearing capacity of foundation on rock.....	15
2.1 Bearing capacity according to ÖNORM.....	15
2.1.1 Die ÖNORM B1997-1-2:2021-08.....	15
2.1.2 Die ÖNORM B1997-1-2: Appendix B.....	15
2.2 Bearing capacity of Foundation on intact rock	18
2.3 Bearing capacity of foundation on fractured rock	20
2.3.1 Hoek-Brown strength criterion.....	22
2.3.2 Bell solution.....	26
2.4 Bearing capacity of foundation on jointed rock.....	27
2.4.1 JOINTED ROCK MASS.....	27
2.4.2 Joints.....	27
2.4.3 Jointed rock properties.....	27
2.4.4 Load distribution in jointed rock.....	28
2.4.5 Bearing capacity according analytical solution Ladanyi and Roy....	30
2.5 Bearing capacity of foundation on layered rock	32
2.6 Material model.....	33
2.6.1 Elasticity modulus	33
2.6.2 Poisson's ratio	34
2.7 Failure criteria	35

2.7.1 Mohr-Coulomb.....	35
2.7.2 Hoek-Brown model	36
2.7.2.1 Disturbance factor.....	38
2.7.2.2 Geological strength index-GSI	38
2.8 Rock and rock mass parameters.....	40
3 Analytical Solution.....	42
3.1 Bearing capacity according to theory Ladanyi and Roy.....	42
3.2 Bearing capacity for joint set 1, $\psi_1/\psi_2 = 60/30$	43
3.3 Bearing capacity for joint set 2, $\psi_1/\psi_2 = 70/20$	43
3.4 Bearing capacity for joint set 3, $\psi_1/\psi_2 = 50/40$	44
4 Numerical model.....	45
4.1 3DEC.....	45
4.2 Modeling.....	46
4.2.1 Model with 2 joint set	49
4.2.1.1 Failure model with 2 joint sets	50
4.2.2 Model with 3 joint set	51
4.2.2.1 Failure model with 3 joint sets	52
5 Result	53
5.1 Bearing capacity numerical model with 2 joint set.....	53
5.2 Bearing capacity numerical model with 3 joint set.....	56
5.2.1 Wedge failure for joint sets 1, $\psi_1/\psi_2 = 60/30$	56
5.2.2 Wedge failure for joint sets 2, $\psi_1/\psi_2 = 70/20$	57
5.2.3 Wedge failure for joint sets 3, $\psi_1/\psi_2 = 50/40$	59
5.2.4 The impact of joint set orientation on bearing capacity	60
5.3 New approach in reverse calculations between DEM and analytical method	61
6 Interpretation and comparison of the results.....	65

6.1 Comparison of the results of the analytical methods with numerical model (DEM) with 2 joint set	65
6.2 Comparison of the results of the analytical methods with numerical model (DEM) with 3 joint set	66
6.2.1 Joints set 1, $\psi_1/\psi_2 = 60/30$	66
6.2.2 Joints set 2, $\psi_1/\psi_2 = 70/20$	67
6.2.3 Joints set 3, $\psi_1/\psi_2 = 50/40$	68
7 SUMMARY	69
8 List of literature	71
9 List of standards	74
10 List of figures	74
11 List of tables	78

1 Introduction

1.1 Methods of assessing the bearing capacity of the foundation on rock

All structures built on the ground, such as buildings, bridges, embankments, etc., consist of two main parts. One of these parts is the superstructure, which is the visible part of the structure, and the second part is the substructure, which is the buried part. The infrastructure is an intermediary between the superstructure and the ground, and it supports the load of the superstructure and brings it to the ground. The lowest part of the structure (including structural elements and the underlying soil) is called the foundation, which transfers forces and moments from the superstructure and its loads to the underlying environment. To secure the foundation, its settlement due to the loads should be allowed and shear failure should not occur. [1]

If a structure is placed on a rock foundation as opposed to an earth foundation, the relevant conditions will change. There are two major differences between rock and soil structure. First, rocks have a greater ability to bear heavier loads than soil, and the discontinuities in the stones cause a different resistance than the rocks without discontinuities, considering that the rocks have good compressive and tensile strength, it is possible to construct light to medium buildings on a rock foundation. But for heavy and semi-heavy structures, different conditions prevail. In this case, the discontinuity in the rock mass may cause sliding and failure of the foundation, or the settlement perpendicular to the joints may cause the overall settlement of the structure. [2]

Despite extensive research conducted in recent decades and focusing on the strength of rock masses and shallow foundations, there are still challenges in the formulation and accurate description of foundation failure mechanisms. Slip and deformation along the discontinuities, as well as deformation and failure in intact parts of the rock mass (blocky regions), make the behavior of rock masses very complex. Therefore, analyzing its load-bearing capacity is a

very complicated task. In the last two decades, with the gradual progress of rock mechanics, efforts have been made to determine the exact bearing capacity of rock masses. [3]

In recent decades, a lot of progress has been achieved in the use of numerical methods and models in rock mechanics, and researchers have had a lot of motivation in this field. [4] Although some numerical models cannot achieve a complete solution, but with the use of sensitivity analysis methods, it is possible to establish a relationship between different parameters. [5] These numerical models include the boundary element method, finite element method, discrete element method, and finite difference method. In addition, different material models in the relevant software make it easier to analyze and allow researchers to pay attention to the properties of discontinuities when analyzing the behavior of rocks.

The existing methods to estimate the bearing capacity and deformability of fractured rock masses are classified into two categories: direct and indirect methods. Direct methods include laboratory tests and in situ tests. The results of laboratory tests on samples with very small cracks and discontinuities due to the inability to include the full range of discontinuity sizes in these small samples have been very different from the results of large-scale block samples. Therefore, indirect methods are chosen to simulate real failure conditions. Indirect methods are classified into three experimental, analytical, and numerical modeling methods.

1.1.1 Experimental Method

Experimental methods have been proven based on empirical correlations, which include the estimation of the bearing capacity of rock masses. [6] In this approach, the characteristics of the rock mass are combined with one of the classification indices that indicate its quality. Since the results of all classification indices include quantitative and qualitative parameters, the mechanical behavior of heterogeneous and scale-dependent discontinuity networks cannot be shown. These methods are usually based on the results of field tests that have been carried out in different construction sites. According to the description method, the classification systems are divided into qualitative and quantitative categories. Qualitative systems are

descriptive, such as the Geologic Strength Index (GSI), but quantitative systems are numerical, such as Q, RMR, RSR, and RQD. [9]

1.1.2 Analytical Method

In analytical methods, a rock mass is considered as a combination of healthy and fractured rock. In these methods, the behavior of the rock mass is checked according to the mathematical relationship of stress and discontinuity according to the sum of the behavior of each component. These methods are concluded according to simple continuous discontinuous systems with infinite stability, fixed distance, and specific orientation. However, in real conditions, the lengths of discontinuities are finite and their geometrical parameters inherently have a statistical distribution. Also, interactions between discontinuities are not considered in these methods. Therefore, in most cases, there are difficulties in convincing the assumptions of these models, especially when we are dealing with a complex rock mass.

1.1.3 Numerical Method

The experimental and analytical methods used to estimate the bearing capacity face uncertainties due to the natural and unpredictable behavior of rock masses, which are significantly affected by the complex network of discontinuities. Therefore, it is important to choose the appropriate numerical method, suitable for the specific conditions and the available equipment, which is associated with the least amount of uncertainty, and in this way, reliable results can be obtained in the basic tasks of rock engineering. [7]

Due to the successive advances in calculations, numerical methods have been given much attention in the analysis of various problems. The most important goal of using numerical methods in fractured rock masses has been modeling based on real conditions, considering the complex and irregular geometry of discontinuities, interactions between discontinuities and blocks, and using complex behavioral models for sound rocks and discontinuities. This advantage gives more confidence to numerical methods than other experimental and analytical methods for extracting mechanical parameters equivalent to rock mass. [7]

The two primary approaches in computational geomechanics aimed at simulation fractured materials are:

1.1.3.1 Discontinuity Modeling Techniques

This Method included Discrete Displacement Analysis (DDA) that explicitly models the discontinuous nature of the material, Discrete Element Method (DEM) that models the discontinuities using independent discrete elements.

In discontinuous methods rock masses consist of separate blocks and separate discontinuity systems, and their interaction and relationship have a major impact on the mechanical behavior of rock masses. Because discontinuity systems introduce discontinuity systems as well as detail into discrete models, these are considered more appropriate methods. However, there is also a dimensionality problem in this method, as it requires high-speed computers with powerful processing capabilities and memory to represent the blocks and discontinuities separately. Therefore, despite the comprehensiveness of the discrete method, it is not very effective for solving certain challenging problems [8].

1.1.3.2 Continuous Modeling Techniques

It is Implementation in Finite Element Method (FEM) and Finite Difference Method (FDM), these two continuous environment approaches are equivalent environments that we use to numerically simulate the mechanical behavior of discontinuous rock masses. In the continuous environment approach, we express the macro-scale behavior of rock mass discontinuities using the principles of continuous environment mechanics, as long as the structural relationships and dependent parameters are maintained based on the fundamental principles of continuous mechanics. [8]

And as can be seen from the Table 1, the advantage and limitation of both methods can be seen in summary.

Table1. Numerical methods of analysis [10]

Analysis method	Critical input parameters	Advantages	Limitations
Continuum modelling (e.g., finite element, finite difference)	Representative slope geometry; constitutive criteria (e.g., elastic, elasto-plastic, creep, etc.); groundwater characteristics; shear strength of surfaces; <i>in situ</i> stress state.	Allows for material deformation and failure, including complex behaviour and mechanisms, in 2-D and 3-D with coupled modelling of groundwater. Can assess effects of critical parameter variations on instability mechanisms. Can incorporate creep deformation and dynamic analysis. Some programs use imbedded language (e.g., FISH) to allow user to define own functions and subroutines.	Users should be well trained, experienced, observe good modelling practice and be aware of model/software limitations. Input data generally limited and some required inputs are not routinely measured. Sensitivity analyses limited due to run time constraints, but this is rapidly improving.
Discontinuum modelling (e.g., distinct element, DDA)	Slope and discontinuity geometry; intact constitutive criteria (elastic, elasto-plastic, etc.); discontinuity stiffness and shear strength; groundwater and <i>in situ stress</i> conditions.	Allows for block deformation and movement of blocks relative to each other. Can model complex behaviour and mechanisms (combined material and discontinuity behaviour, coupled with hydro-mechanical and dynamic analysis). Able to assess effects of parameter variations on instability. Some programs use imbedded language (e.g., FISH) to allow user to define own functions and subroutines.	As above, experienced users needed. General limitations similar to those listed above. Need to simulate representative discontinuity geometry (spacing, persistence, etc.). Limited data on joint properties available (e.g., joint stiffness, j_{k_n} and j_{k_s}).

2 Bearing capacity of foundation on rock

2.1 Bearing capacity according to ÖNORM

2.1.1 Die ÖNORM B1997-1-2:2021-08

On the other hand in the ÖNORM B 1997-1-2, Design, calculation and dimensioning in geotechnics - Part 2: Surface foundations - includes the proof of load-bearing capacity for the failure mechanisms - mechanical ground failure (GEO), - sliding (GEO) and eccentric loading (toppling) as well as the proof of serviceability (settlement, settlement differences and twisting). In this ÖNORM, foundations in rock are only covered in normative appendix B.

2.1.2 Die ÖNORM B1997-1-2: Appendix B

According to the figure1 in this appendix can be found the Characteristic values of bearing capacity

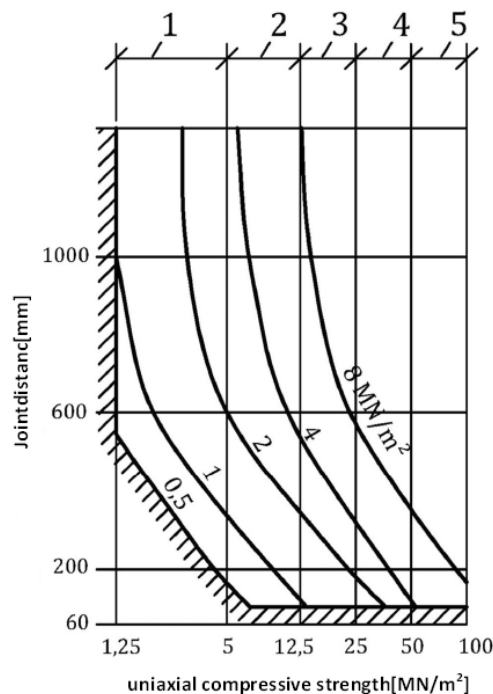


Figure1. Characteristic values for bearing capacity from ÖNORM B1997-1-2 Figure B.1

As shown in the diagram, we can easily use the uniaxial compressive strength of the rock and the distance between the joints to determine the bearing capacity of a foundation. For example, for a rock with a uniaxial compressive strength of 5 [MN/m²] and a joint spacing of 600 [mm], we obtain the foundation's permissible bearing capacity of 2[MN/m²]. But it should be noted that this diagram does not give us information about the orientation of the set of the joint sets, their quantity and their normal and shear strength. Therefore, such charts may sometimes produce incorrect results, but they can give background information to the designer. According to the relevant standard, must always be determined by a geotechnical expert with relevant experience if at least one of the following points applies:

- The classification of the subsoil as rock is unclear.
- Geologically complex conditions exist.
- The rock is strongly fractured, disturbed, or sensitive to weathering.
- The subsoil consists of variably firm rock.
- The rock surface has a slope of more than 20%.
- Situations according to B.2 to B.4 are present. (Figure2-4)
- If rocks contain lime, gypsum, anhydrite, Salt, or expansive clay minerals, swelling or dissolution phenomena are to be expected.

In special spatial arrangements of discontinuity or when the foundation is close to a rock edge, the ÖNORM specifies the following cases:

B2:

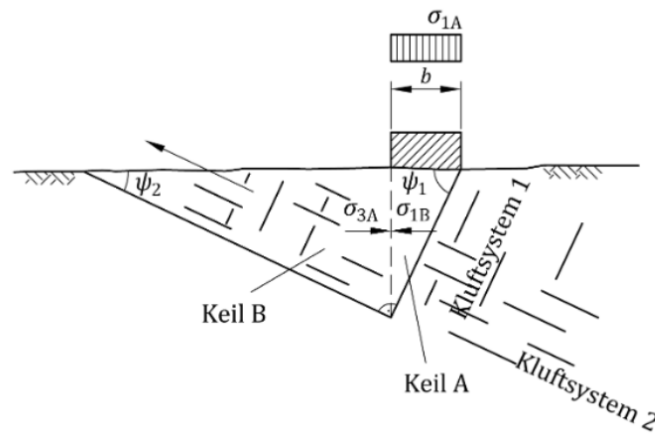


Figure2. Bearing capacity of a foundation on rock with inclined, approximately orthogonal joint systems (show Wyllie [11]) from ÖNORM B1997-1-2, Appendix B

B3:

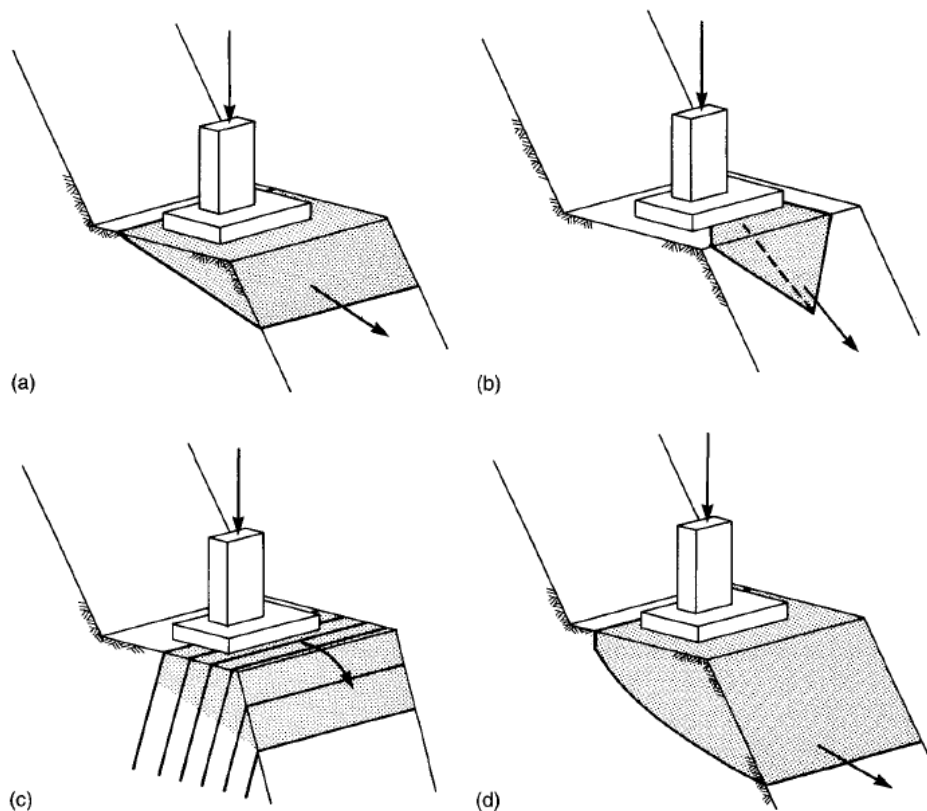


Figure3. Failure mechanisms (a) planar sliding failure on single discontinuity; (b) wedge sliding failure on two intersecting discontinuities; (c) toppling failure of steeply dipping slabs; (d) circular failure in closely fractured rock (Wyllie [11]) from ÖNORM B1997-1-2, Appendix B

B4:

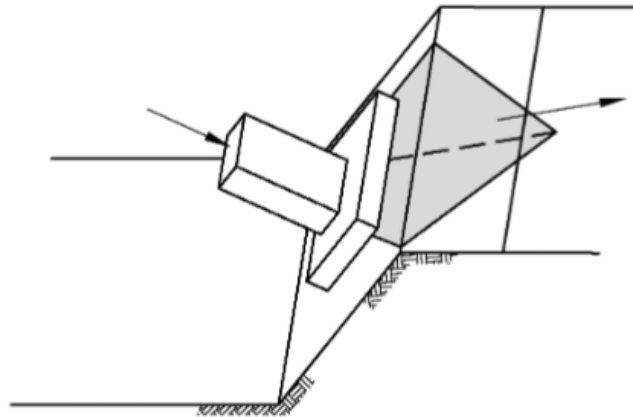


Figure4. Example of the translation of a wedge-shaped sliding body on a horizontal rock surface (show Wyllie [11]) from ÖNORM B1997-1-2, Appendix B

2.2 Bearing capacity of Foundation on intact rock

The bearing capacity of intact rock is referred to as a rock mass with a normal discontinuity spacing of more than four to five times the width of the foundation. In the corresponding rule, the joints are far apart so that the orientation and position of the joint is not important. [12]

The first studies on the bearing capacity of stone have been carried out by Rochester regarding rock. The rocks are divided into three groups, soft, medium and hard, with a bearing capacity of 1.4, 2.4 and 4.8[MPa]. Also, it is explained about the structures and their improvement methods. [11]

Table2. Bearing capacity, Settlement intact rock [11]

Rock is classified as:	<i>Seamy rock:</i> (11/29/60)
<i>Soft rock:</i> Clinton and Queenstown shale <i>Medium rock:</i> Rochester shale <i>Hard rock:</i> Lockport dolomite and Medina sandstone	If seams of rock or soil having little or no bearing value occur within the 1.5 m (5 ft) depth below a bearing area*:
If a hole below the bearing surface passes through at least 1.5 m (5 ft) of rock, the bearing capacity shall be:	<ol style="list-style-type: none"> 1. Seams less than 6 mm (1/4 in) thick may be ignored. 2. Seams 6 to 13 mm (1/4 to 1/2 in) thick occurring deeper than 1 m (3 ft) may be ignored. 3. Seams thicker than 13 mm (1/2 in) and deeper than 1.5 m (5 ft) may be ignored depending upon the discretion of the building inspector. 4. Seams more than 13 mm (1/2 in) thick occurring within a depth of 1.5 m (5 ft), or more than 6 mm (1/4 in) thick in the first 1 m (3 ft) of depth are unsatisfactory. The bearing surface is to be lowered below the bottom of the lowest known seam of thickness greater than 13 mm (1/2 in) and further as required to meet these provisions. A new boring or borings shall be required and any seam occurring in the new borings shall be examined as above. 5. The building inspector may order pressure grouting of seams and tests to establish bearing values of grouted foundations.
<ul style="list-style-type: none"> • 1.4 MPa (30 kips/ft²) in soft rock; • 2.4 MPa (50 kips/ft²) in medium rock; • 4.8 MPa (100 kips/ft²) in hard rock; (providing that all 1.5 m are in the same kind of rock). (10/13/33)	
For buildings less than six stories or 23 m (76 ft) high, the Director of Buildings may reduce the number of drill holes required to be as few as, but not less than, one-fifth of the number of bearing areas, if in his or her opinion the nature and condition of the rock justify such omission. (1/11/66)	

In the table2 bearing capacity is considered based on geological conditions such as rock type and age. The information in this table is based on observations obtained from stable structures built on rock, including safety factors and minimum settlements [9].

movement of shear zones leads to sudden shear failure as depicted in figure 5. [13]

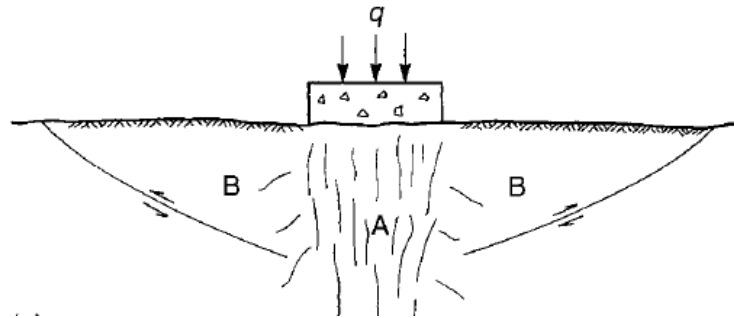


Figure5. Fracture (zone A) and unfractured (zone B) on rock surface [13]

In the presented Mohr diagram (Figure6), the reduction in the strength of the sub-base rock at failure (area A) under the foundation compared to that enclosed by unbroken rock wedges around the foundation (zone B) is displayed.

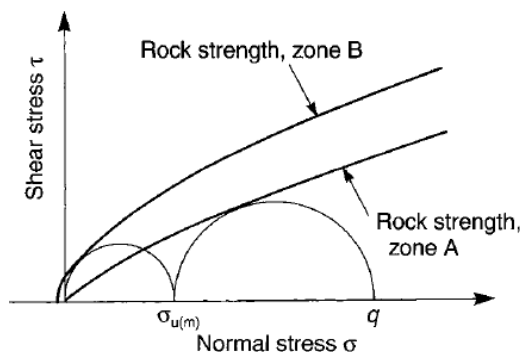


Figure6. Mohr diagram of stresses in bearing rock [13]

As shown in figure 7 the rock under the footing in the state of triaxial compression with the main stress is equal to the bearing pressure (q) and the partial main stress is equal to the limit applied by the surrounding rock.

We calculate the bearing capacity using a method similar to soil mechanics, which includes the formation of mobile and resistant shear zones. In this regard, shear strength parameters are related to fractured rocks or fault surfaces that include the edges of fracture zones and are detected by geological studies. According to this method, the fracture lines are considered as straight lines and the shear zones A and B are made according to the figure.

This method is suitable for an infinite foundation placed on a horizontal rock surface. The condition of the rock under the foundation is considered similar to a triaxial test, in which the main stress in area A is equal to the pressure applied to the foundation, and we ignore the weight of the stone on the foundation. Zone B is also similar to a triaxial test where the main stress is mainly horizontal. The maximum amount of stress that the surrounding rock can withstand is the uniaxial compressive strength of the rock mass $\sigma_{u(m)}$ in area B, and assuming that the footing is at the ground surface. [13]

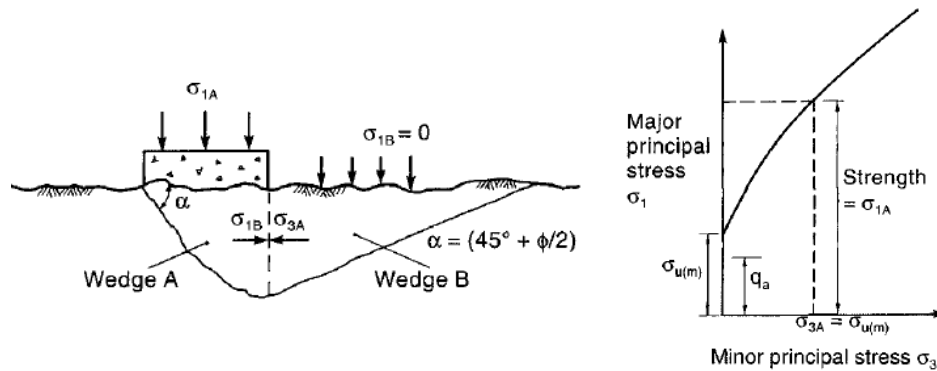


Figure 7. Analysis of bearing capacity of fractured rock [13]

2.3.1 Hoek-Brown strength criterion

According to Hoek-Brown theory, the strength of fractured rock mass is:

$$\sigma_1 = (m \sigma_{u(r)} \cdot \sigma_3 + s \sigma_{u(r)}^2)^{0.5} + \sigma_3 \quad (2.1)$$

And m and s are Hoek's constants, which are influenced by both the rock type and discontinuity characteristics. The specific values for m and s are consolidated in table 4, $\sigma_{u(r)}$ is the unconfined compressive strength of intact rock, and σ_1 and σ_3 are the principal and minor principal stresses, respectively. [14]

The uniaxial compressive strength of a fractured rock mass is as follows:

$$\sigma_{u(m)} = (s \sigma_{u(r)}^2)^{0.5} \quad (2.2)$$

Which is equal to σ_3 and in this case the bearing capacity is equal to the main stress in area A and is equal to:

$$\sigma_1 = s^{0.5} \sigma_{u(r)} [1 + (ms^{-0.5} + 1)^{0.5}] \quad (2.3)$$

Table 4. Approximate relationship between rock mass quality and material constant [14]

		CARBONATE ROCKS WITH WELL DEVELOPED CRYSTAL CLEAVAGE <i>dolomite, limestone and marble</i>	LITHIFIED ARGILLACEOUS ROCKS <i>mudstone, siltstone, shale and slate (normal to cleavage)</i>	ARENACEOUS ROCKS WITH STRONG CRYSTALS AND POORLY DEVELOPED CRYSTAL CLEAVAGE <i>sandstone and quartzite</i>	FINE GRAINED POLYMINERALLIC IGNEOUS CRYSTALLINE ROCKS <i>andesite, dolerite, diabase and rhyolite</i>	COARSE GRAINED POLYMINERALLIC IGNEOUS & METAMORPHIC CRYSTALLINE ROCKS <i>amphibolite, gabbro gneiss, granite, norite, quartz-diorite</i>
INTACT ROCK SAMPLES						
<i>Laboratory size specimens free from discontinuities</i>	m	7.00	10.00	15.00	17.00	25.00
	s	1.00	1.00	1.00	1.00	1.00
*CSIR rating: RMR = 100						
†NGI rating: Q = 500						
VERY GOOD QUALITY ROCK MASS						
<i>Tightly interlocking undisturbed rock with unweathered joints at 1–3 m</i>	m	2.40	3.43	5.14	5.82	8.56
	s	0.082	0.082	0.082	0.082	0.082
CSIR rating: RMR = 85						
NGI rating: Q = 100						
GOOD QUALITY ROCK MASS						
<i>Fresh to slightly weathered rock, slightly disturbed with joints at 1–3 m</i>	m	0.575	0.821	1.231	1.395	2.052
	s	0.00293	0.00293	0.00293	0.00293	0.00293
CSIR rating: RMR = 65						
NGI rating: Q = 10						
FAIR QUALITY ROCK MASS						
<i>Several sets of moderately weathered joints spaced at 0.3–1 m</i>	m	0.128	0.183	0.275	0.311	0.458
	s	0.00009	0.00009	0.00009	0.00009	0.00009
CSIR rating: RMR = 44						
NGI rating: Q = 1						
POOR QUALITY ROCK MASS						
<i>Numerous weathered joints at 30–500 mm, some gouge. Clean compacted waste rock</i>	m	0.029	0.041	0.061	0.069	0.102
	s	0.000003	0.000003	0.000003	0.000003	0.000003
CSIR rating: RMR = 23						
NGI rating: Q = 0.1						
VERY POOR QUALITY ROCK MASS						
<i>Numerous heavily weathered joints spaced <50 mm with gouge. Waste rock with fines</i>	m	0.007	0.010	0.015	0.017	0.025
	s	0.0000001	0.0000001	0.0000001	0.0000001	0.0000001
CSIR rating: RMR = 3						
NGI rating: Q = 0.01						

*CSIR Council of Scientific and Industrial Research (Bieniawski, 1974).

†NGI Norwegian Geotechnical Institute (Barton *et al.*, 1974).

The permissible bearing pressure q_a is related to the rock mass resistance with the safety factor FS, and the correction factor C_{f1} is equal to:

$$q_a = \frac{\sigma_1 \cdot C_{f1}}{FS} \quad (2.4)$$

To calculate the shape of the foundation to the calculated allowable bearing pressure, we use the coefficient C_{f1} and it includes the values given in the table 5 below, in which L is the length and B is the width [15].

Table5. Correction factors for foundation shapes [15]

<i>Foundation shape</i>	C_{f1}	C_{f2}
Strip ($L/B > 6$)	1.0	1.0
Rectangular		
$L/B = 2$	1.12	0.9
$L/B = 5$	1.05	0.95
Square	1.25	0.85
Circular	1.2	0.7

The strength of intact rock $\sigma_{u(r)}$ is determined based on laboratory tests on rock cores, while for fractured rock we define the strength through the above equation along with the fracture degree of the rock mass with the constants m and s. We can measure the compressive strength of intact rock using a compression device or point load tester. The following table 6 is used as a good reference for the uniaxial strength of intact rock. [16]

Table6. Classification of rock material strengths [16]

Grade	Description	Field identification	Approximate range of compressive strength	
			MPa	(p.s.i)
R6	Extremely strong rock	Specimen can only be chipped with geological hammer	>250	(>36 000)
R5	Very strong rock	Specimen requires many blows of geological hammer to fracture it	100–250	(15 000–36 000)
R4	Strong rock	Specimen requires more than one blow with a geological hammer to fracture it.	50–100	(7 000–15 000)
R3	Medium weak rock	Cannot be scraped or peeled with a pocket knife; specimen can be fractured with single firm blow of geological hammer	25–50	(3 500–7 000)
R2	Weak rock	Can be peeled with a pocket knife; shallow indentations made by firm blow with point of geological hammer	5–25	(725–3 500)
R1	Very weak rock	Crumbles under firm blows with point of geological hammer; can be peeled by a pocket knife	1–5	(150–725)
R0	Extremely weak rock	Indented by thumbnail	0.25–1	(35–150)
S6	Hard clay	Indented with difficulty by thumbnail	>0.5	(>70)
S5	Very stiff clay	Readily indented by thumbnail	0.25–0.5	(35–70)
S4	Stiff clay	Readily indented by thumb but penetrated only with great difficulty	0.1–0.25	(15–35)
S3	Firm clay	Can be penetrated several inches by thumb with moderate effort	0.05–0.1	(7–15)
S2	Soft clay	Easily penetrated several inches by thumb	0.025–0.05	(4–7)
S1	Very soft clay	Easily penetrated several inches by fist	<0.025	(<4)

2.3.2 Bell solution

This solution works based on Terzaghi's theory and for weak rock with low fracture, it has an expression for the permissible bearing capacity of Bell's solution and it is presented using the principles explained above. This analysis is based on the weight bearing capacity of the rock in the active wedge. Bell's solution to the allowable bearing capacity for strip footings is a square or circular solution. [11]

$$q_a = \frac{C_{f1} \cdot c \cdot N_c + C_{f2} \left(\frac{B \cdot \gamma_r}{2} \right) N_\gamma + \gamma D N_q}{FS} \quad (2.5)$$

Where B represents the width (for strip or square footing) or diameter (for circular footing), γ_r denotes the rock density. Additionally, D represents the depth of embedment, while c and φ stand for the cohesion and friction angle of the rock mass, respectively.

The correction factors C_{f1} and C_{f2} which account for the footing shape are given in above Table 5. The terms N_c , N_γ and N_q are bearing capacity factors defined as follows [17]

$$N_c = 2N_\varphi^{1/2}(N_\varphi + 1) \quad (2.6)$$

$$N_\gamma = 0.5N_\varphi^{1/2}(N_\varphi^2 - 1) \quad (2.7)$$

$$N_q = N_\varphi^2 \quad (2.8)$$

$$N_\varphi = \tan^2(45 + \varphi/2) \quad (2.9)$$

The factor N_c shows the influence of the cohesion, the factor N_γ shows the influence of the weight of rock in the foundation, and the factor N_q shows the influence of the surcharge and FS is the factor of safety.

2.4 Bearing capacity of foundation on jointed rock

2.4.1 JOINTED ROCK MASS

Due to the existence of discontinuity in the rock mass, the issue in the rock mechanics has been considered as a different issue [18]. The ingredients of raw stones have been subjected to thermal, mechanical and chemical activity for millions of years. As a result, discontinuities caused by geological events have been created at different times and have resulted in different stress states in the rock [19]. The factor or process that created these discontinuities has a great impact on the geometric and mechanical properties of the discontinuities. Therefore, as emphasized, understanding the formation method of discontinuities, through understanding the earth's structures, is of particular importance. [20].

In general, we divide discontinuity appearance factors into four groups: tectonic factors, residual stresses, shrinkage due to cooling or drying, and lastly, ground surface movements.

2.4.2 Joints

The most common and generally the most important geotechnical discontinuities in rocks are joints. Joints are usually regularly spaced depending on the mechanical properties of the individual rocks or the thickness of the layer involved. Joints are generally located in a set (joint set) where each set is made up of parallel joints. Joints are the most important factor that controls the deformation, resistance and permeability of the rock mass. [21]

2.4.3 Jointed rock properties

The International Society for Rock Mechanics has mentioned ten important parameters to describe the characteristics of discontinuities (joints). You can see these parameters schematically in figure 8, which includes the characteristics of discontinuity within the rock mass. The most important features include orientation, distance and frequency, durability, roughness, wall strength, filling, seepage and block size.

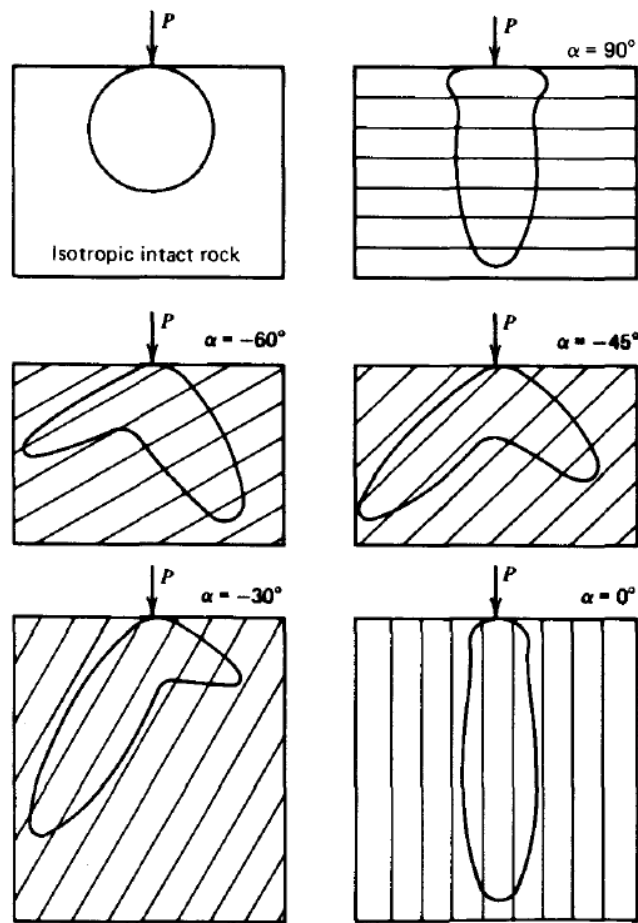


Figure9. Numerically determined lines of equal stress ($\sigma = \text{const.}$) in an anisotropic, elastic and homogeneous half-space (plane distortion state. i.e. the loads are line loads) [9]

John Bray shows that for the special condition that a line load has been decomposed into X and Y components parallel and perpendicular to the planes of discontinuity (Figure 10), the stress distribution in the rock is still completely radial. [23]

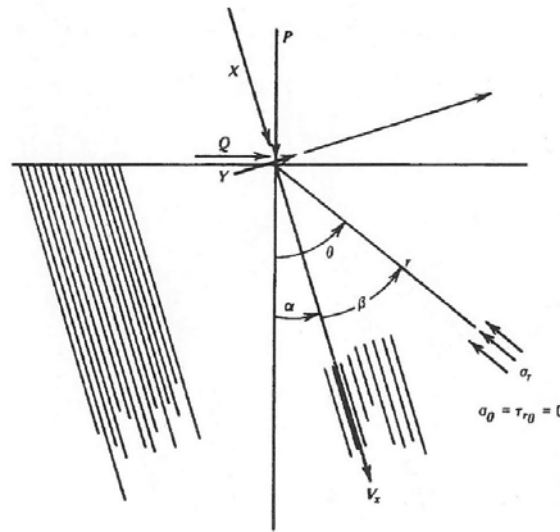


Figure 10. Load distribution in the anisotropic (transversely isotropic), elastic and homogeneous continuum [9]

$$\sigma_r = \frac{h}{r \cdot \pi} \left[\frac{X \cos \beta + Y \sin \beta}{(\cos^2 \beta - g \sin^2 \beta)^2 + h^2 \sin^2 \beta \cos^2 \beta} \right] \quad (2.10)$$

$$g = \sqrt{1 + \frac{E}{(1-\nu^2)k_n s}} \quad (2.11)$$

$$h = \sqrt{\left(\frac{E}{(1-\nu^2)} \right) \left[\frac{2(1+\nu)}{E} + \frac{1}{k_s s} \right] + 2 \left(g - \frac{\nu}{(1-\nu)} \right)} \quad (2.12)$$

Here is E is E-modulus and ν is Poisson's ratio of the rock and s is joint distance and k_n and k_s are normal and shear stiffness of the joint. [24], [9]

2.4.5 Bearing capacity according analytical solution Ladanyi and Roy

In the situation where the rock has two sets of joints perpendicular to each other, we cannot use the above relationships to determine the bearing capacity. To calculate the bearing capacity in fractured rock, a passive rock wedge is created in the failure mechanism, which creates a confining stress on the active rock wedge under the footing. The amount of this confining stress is based on the influence of the strength of the rock mass, which consists of unbroken rock or interconnected pieces of unbroken rock. [11]

But if there are discontinuity sets that form one or more surfaces of this wedge, the bearing capacity of the foundation may be reduced due to two specific factors.

First, we determine the shape of the wedge based on the orientation of the discontinuities, and the dimensions and surface of the wedge can be limited. Second, the strength of the discontinuities is usually significantly lower than the rock mass, and in this case, the failure of the foundation may occur due to the displacement of the inactive wedge.

As this situation is shown in the figure 11, the rock mass contains two sets of conjugate joints dipping at angles ψ_1 and ψ_2 , which form the base surfaces of an active wedge (A) and a passive wedge (B), respectively. [13]

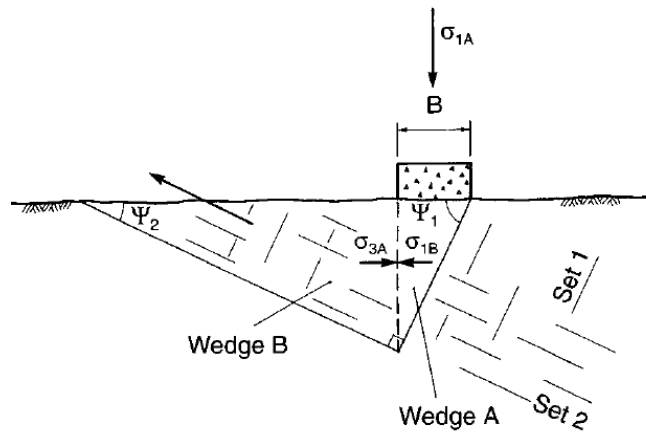


Figure11. Foundation on rock containing inclined bedding planes and orthogonal joint sets [13]

In this analytical solution to determine the minimum horizontal principal stress, σ_{3A} acting on active wedge A, and the allowable bearing capacity, q_a , use the subsequent equation for calculation.[13]

$$\sigma_{3A} = \left(\frac{\gamma B}{2 \tan \psi_1} \right) N_{\varphi_2} + \left(\frac{c_2}{\tan \varphi_2} \right) (N_{\varphi_2} - 1) \quad (2.13)$$

$$q_a = \frac{[\sigma_{3A} N_{\varphi_1} + (c_1 / \tan \varphi_1) (N_{\varphi_1} - 1)]}{FS} \quad (2.14)$$

$$N_{\varphi_1} = \tan^2 \left(45 + \frac{\varphi_1}{2} \right) \quad (2.15)$$

$$N_{\varphi_2} = \tan^2 \left(45 + \frac{\varphi_2}{2} \right) \quad (2.16)$$

Let B represent the footing width, γ denote the rock density and ψ_1 indicate the dip of discontinuity set 1 and c_1 and c_2 are the cohesions of discontinuity sets 1 and 2 respectively. Additionally φ_1 and φ_2 are the friction angles corresponding to discontinuity sets 1 and 2 and FS is the factor of safety. [13]

2.5 Bearing capacity of foundation on layered rock

In situations where a foundation rests on a thin layer of strong rock above a significant thickness of significantly weaker rock, three modes of failure according to figure 12 may occur. The foundation may pass through the stronger top layer, or the top layer may fail through buckling or bending. In all three of these situations, the failure of the upper rock layer will probably result in a sudden and significant settlement of the foundation, especially if the material in the lower layer has a limited load-bearing capacity. [25]

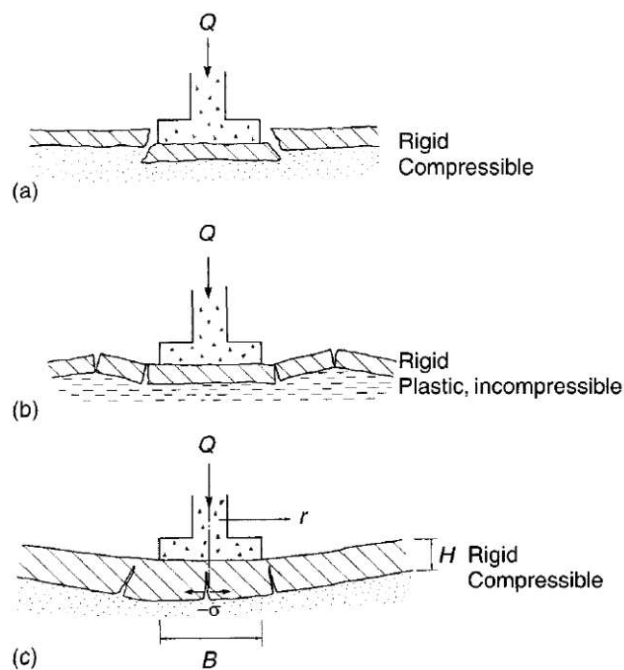


Figure 12. Spread footings on layered rock formations (a) punching failure, (b) buckling failure, and (c) bending failure. [25]

Because the upper layer of rock has a significantly higher modulus than the lower layer, most of the load is imposed on the upper layer and the stability of the foundation mainly depends on the capacity of this layer. In the initial stages of design, we consider that the top layer can bear the entire load, because then a conservative design is obtained. But if we can accurately

determine the deformation modulus of both materials, we can determine the stress distribution between the layers more accurately and, if necessary, make changes in the foundation plan. [11]

The failure mechanism of the upper layer depends on the following two things: the characteristics of the rock mass of each layer and the ratio of the thickness of the upper layer (H) to the width of the base (B). If the H/B ratio is low and the bottom layer is compressible, such as weathered or porous rocks, a punch-type failure is likely to occur. But if the underlying layer is plastic and incompressible, such as clay or soft shale, the upper layer may face buckling. [25]

For larger values of H/B ratio, and in conditions where the lower layer is compressible, the upper layer may fail through bending. [11]

2.6 Material model

All the calculations that are done using a numerical program are based on the model of the material on which the calculation is based, which in fact the calculation is based on this model. These material models are mathematically formulated based on experiments and observations that describe the behavior between loads and deformations [26].

For rock modeling, the determination of stresses, deformations, safety factors, and bearing capacity involves the use of either the Mohr-Coulomb model or the Hoek-Brown calculation model. Both of these are associated with special features that are discussed in the respective chapters.

2.6.1 Elasticity modulus

The modulus of elasticity or Young's modulus of a material describes the stress-strain relationship. In Rock Mechanics and Tunnel Construction determine the linear behavior region of the unloading loop and then consider the ratio of stress change to change in deformation. [27]

$$E = \frac{\Delta\sigma}{\Delta\varepsilon} \quad (2.17)$$

The modulus of elasticity is of great importance, especially in deformation calculations. It should be noted that under normal conditions, the modulus of elasticity may change based on the desired direction. In Table 7, typical rock parameters of intact isotropic rocks are presented.

Table 7. Common elastic constants for intact rock [11]

Rock Type	E-Modul [GPa]	Poisson's ratio	Reference
Andesite, Nevada	37,0	0.23	Brandon (1974)
Argillite, Alaska	68,0	0.22	Brandon (1974)
Basalt, Brazil	61,0	0.19	Ruiz (1966)
Coal, USA	3.45	0.42	Ko and Gerstle (1976)
Dolomite, USA	51.7	0.29	Haimson and Fairhurst (1970)
Salt, Ohio	28.5	0.22	Sellers (1970)
Sandstone, Germany	29.9	0.31	van der Vlis (1970)

2.6.2 Poisson's ratio

Poisson's ratio (ν) or transverse strain coefficient represents a unitless material parameter that defines the transverse contraction of a material. Poisson's ratio ranges from 0.00 to 0.50. This value can deduce the horizontal stress from the vertical stress [26]. A Poisson's ratio of 0.00 indicates a material that is not subject to transverse contraction, in fact no horizontal stress is produced by the vertical load. If Poisson's ratio is 0.50, the horizontal stresses are equal in magnitude to the vertical stresses.

$$\sigma_{Horizontal} = \frac{\nu * \sigma_{vertical}}{1 - \nu} \quad (2.18)$$

2.7 Failure criteria

2.7.1 Mohr-Coulomb

In the Mohr-Coulomb material model, there is essentially a fracture criterion. These boundary conditions are described in terms of friction angle " φ " and cohesion " c ". The fracture line is described by the following formula and shown in the figure 13.

$$\tau = \sigma \cdot \operatorname{tg}\varphi + c \quad (2.19)$$

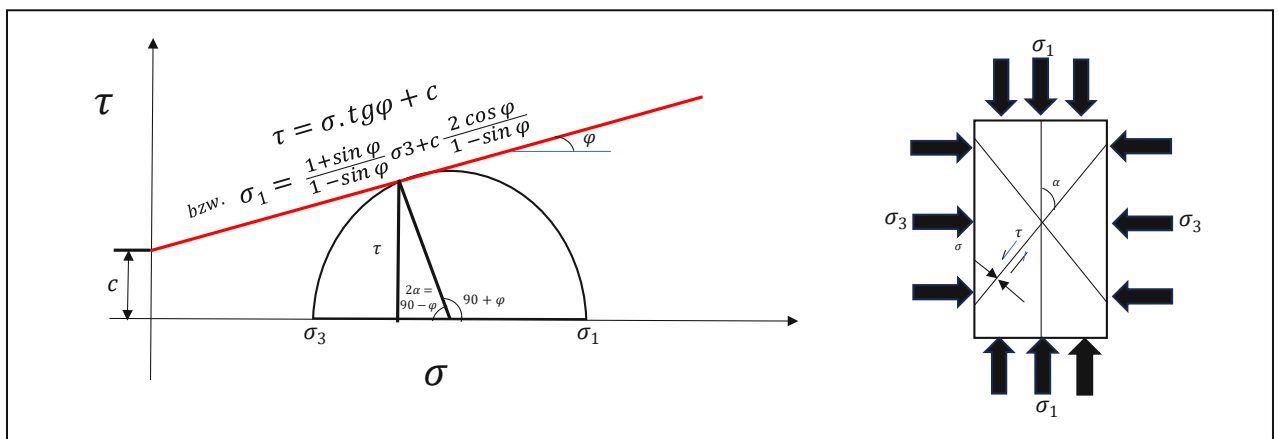


Figure13. Mohr-Coulomb material model [28]

Here, " φ " is the fraction of the shear stress that is dependent on the normal stress (this ratio increases with increasing normal stress) and " c ", is the fraction of the stress which is separate from shear stress. By this criterion, failure is exactly when the largest Mohr's stress circle (defined by the smallest and largest principal normal stress) hits the failure line at point P. [27].

This material model is used because the Mohr-Coulomb material model depends on only two parameters. In addition, both the friction and cohesion angles are determined through testing and are acceptable. [29]

We can determine the angle of friction and cohesion, for example, from uniaxial and triaxial tests. As you can see in figure 14, uniaxial tests are

different from triaxial tests because the principal normal stress σ_3 is zero in the uniaxial compression test. As a result, lower achievable limit stresses are observed in the triaxial test [27].

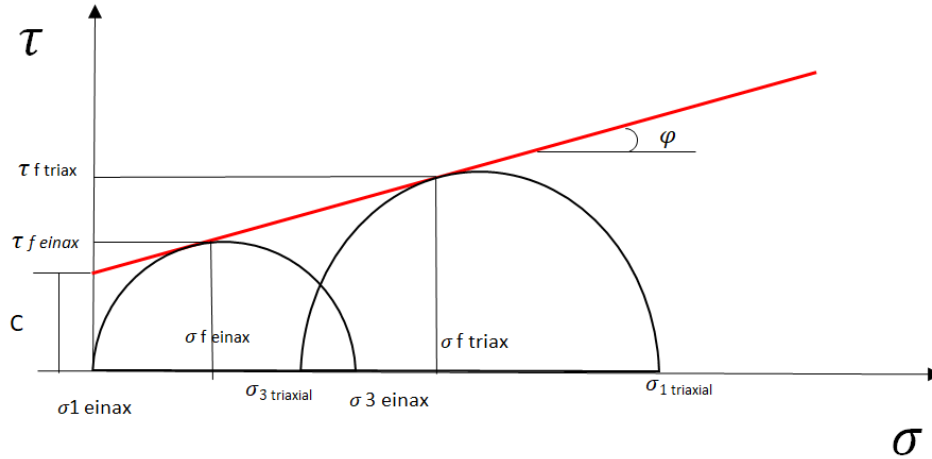


Figure14. Representation of the shear parameters in a uniaxial and triaxial stress state using stress circles [27]

2.7.2 Hoek-Brown model

The Hoek-Brown model is a failure criterion obtained through experimental tests and, like the Mohr-Coulomb model, presents a fracture line (Figure 15). But Hoek and Brown criterion has a parabolic break line. We need the following formulas to define the criteria. [30]

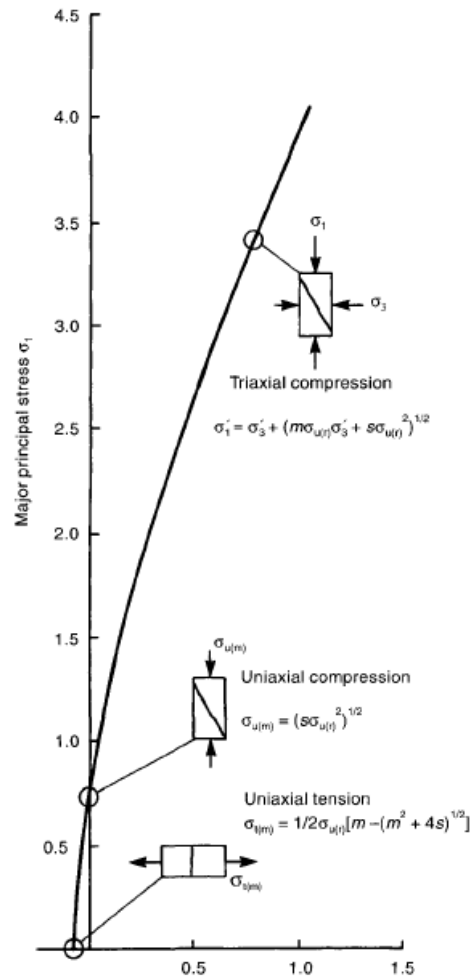


Figure 15. Hoek-Brown material model [31]

$$\sigma_1 = \sigma_3 + \sigma_{ci} * (m_b * \frac{\sigma_3}{\sigma_{ci}} + s)^a \quad (2.20)$$

$$m_b = m_i + \exp * \left(\frac{GSI - 100}{28 - 14D} \right) \quad (2.21)$$

$$s = \exp * \left(\frac{GSI - 100}{9 - 3D} \right) \quad (2.22)$$

$$a = \frac{1}{2} + \frac{1}{6} * \left(e^{\frac{-GSI}{15}} - e^{\frac{-20}{3}} \right) \quad (2.23)$$

As shown in the formulas above, the Hoek-Brown criterion is highly dependent on the Geological Strength Index (GSI). Three of the four input values (m_b , s , a) are directly related to it, and therefore m_b is the Material parameters for Rockmass and m_i is the Material parameters for intact rock. GSI is a purely visual method of estimating parameters and has much more scope for interpretation and therefore more scope for variation in a safety

calculation. For the reasons mentioned and because there is a high probability of significant change in the results and at the same time minimal change in the input parameters (positive as well as negative), the Mohr-Coulomb model is preferred in this work. [30]

2.7.2.1 Disturbance factor

D is a factor in the Hoek-Brown criterion that represents blast damage or existing faults due to careless demolition of rock. These figures and numbers are usually specified through tables or empirical values and should only be used in the vicinity of the damaged rock surface. The value of D is between 0 (no previous damage) and 1 (severe damage) [32].

2.7.2.2 Geological strength index-GSI

GSI (geological strength index) is the same value presented by Hoek to estimate the strength parameters of a rock mass. GSI is determined completely visually and does not rely on physical measurements [33]. We compare the mass of rock that is evaluated with the diagram. As shown in figure 16, we divide the diagram horizontally according to the degree of roughness or weathering of the discontinuities, and the rock structure is examined vertically. The GSI has a value range from 0 (very poor) to 100 (very good).

GEOLOGICAL STRENGTH INDEX FOR JOINTED ROCKS (Hoek and Marinos, 2000)
 From the lithology, structure and surface conditions of the discontinuities, estimate the average value of GSI. Do not try to be too precise. Quoting a range from 33 to 37 is more realistic than stating that GSI = 35. **Note that the table does not apply to structurally controlled failures.** Where weak planar structural planes are present in an unfavourable orientation with respect to the excavation face, these will dominate the rock mass behaviour. The shear strength of surfaces in rocks that are prone to deterioration as a result of changes in moisture content will be reduced if water is present. When working with rocks in the fair to very poor categories, a shift to the right may be made for wet conditions. Water pressure is dealt with by effective stress analysis.








STRUCTURE	SURFACE CONDITIONS				
	DECREASING SURFACE QUALITY →				
 INTACT OR MASSIVE - intact rock specimens or massive in situ rock with few widely spaced discontinuities	VERY GOOD Very rough, fresh unweathered surfaces	GOOD Rough, slightly weathered, iron stained surfaces	FAIR Smooth, moderately weathered and altered surfaces	POOR Slickensided, highly weathered surfaces with compact coatings or fillings or angular fragments	VERY POOR Slickensided, highly weathered surfaces with soft clay coatings or fillings
DECREASING INTERLOCKING OF ROCK PIECES ↓	 INTACT OR MASSIVE - intact rock specimens or massive in situ rock with few widely spaced discontinuities	90	80	N/A	N/A
	 BLOCKY - well interlocked undisturbed rock mass consisting of cubical blocks formed by three intersecting discontinuity sets		70		
	 VERY BLOCKY - Interlocked, partially disturbed mass with multi-faceted angular blocks formed by 4 or more joint sets		60	50	
	 BLOCKY/DISTURBED/SEAMY - folded with angular blocks formed by many intersecting discontinuity sets. Persistence of bedding planes or schistosity			40	30
	 DISINTEGRATED - poorly interlocked, heavily broken rock mass with mixture of angular and rounded rock pieces				20
	 LAMINATED/SHEARED - Lack of blockiness due to close spacing of weak schistosity or shear planes	N/A	N/A		10

Figure16. Geological strength index for jointed rock masses [34]

2.8 Rock and rock mass parameters

We have to differentiate between intact rock or rock material and rock mass. Intact rock is a continuum or polycrystalline solid between discontinuities consisting of a collection of minerals or grains. The in-situ ambient rock mass consists of intact rock blocks separated by discontinuities such as joints, bedding planes, folds, shear zones, and faults. [35]

Parameters play the role of essential material constants that we need to describe a material. Elastic modulus, Poisson's ratio, friction angle and cohesion are among the most important parameters. All these parameters are directly or indirectly dependent on each other. Especially when determining rock properties, only large-scale tests can be used, which is the only way to provide an overall picture that includes fracture body properties and rock properties. If it is not possible to perform in-situ tests, we can determine the required rock parameters using uniaxial or triaxial compression tests in the laboratory. [36]

The effect of sample size on compressive strength was evaluated through in situ tests, and you can observe this effect in figure 17. You can see that the uniaxial compressive strength is reduced to about 10% on the large scale. [18]

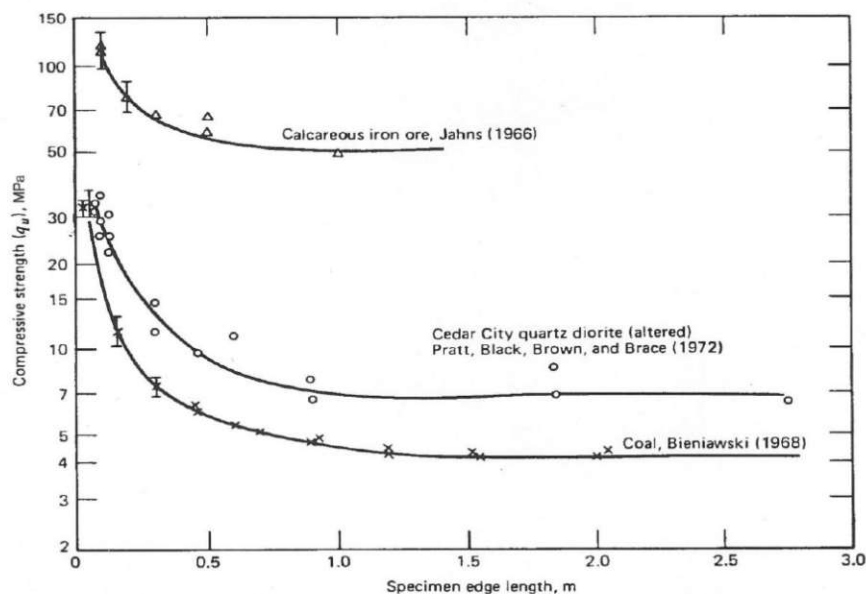


Figure 17. Impact of specimen size on compressive strength [18]

When creating a model for calculating the building subsurface, as figure 18 shows, the area under consideration is very important. If we examine a small section (for specific details), we can consider the rock as an unbroken isotropic continuum. But if we consider a larger area, for example for landslides or slope stabilization, bearing capacity measures, discontinuities should be considered and included.

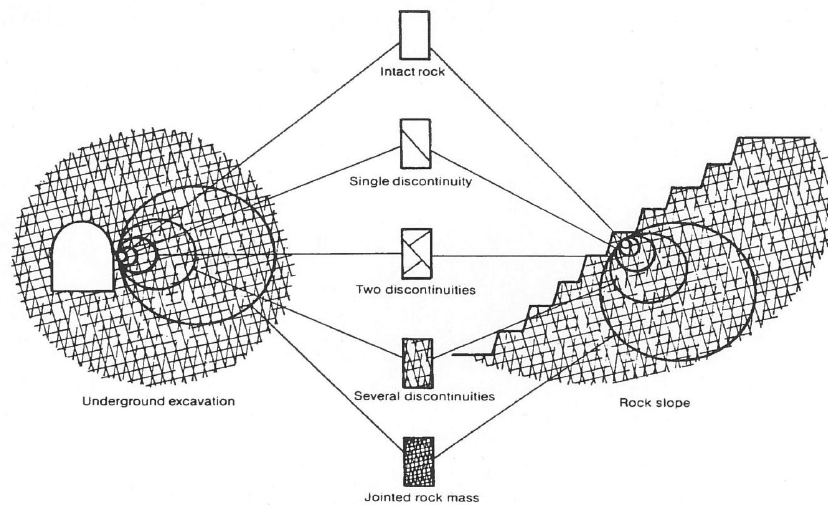


Figure18. Modification of the model properties only by changing the area under consideration

[37]

3 Analytical Solution

3.1 Bearing capacity according to theory Ladanyi and Roy

According to this theory outlined in section 2.4.5 for jointed rocks, failure beneath the foundation is anticipated to occur due to shear failure within the discontinuities. Equations 2-13 to 2-16 were employed in the determination of bearing capacity.

For this purpose, to determine the bearing capacity, we considered a rectangular foundation with dimensions of 1[m]*2[m] on the rock mass with a density of 0.027 [MN/m³], which contains two set of orthogonal discontinuities. [11]

The mechanical characteristics of the joints are identical, and their corresponding values are provided in the table below. To enhance our comprehension of the influence of the joints orientation, friction angle, and cohesion on the foundation's bearing capacity, we have examined three distinct discontinuity orientation states, which are perpendicular to each other. Additionally, various values for friction angles and cohesion have been taken into account, as indicated in the table 8 and 9 below.

Table8. The orientation of the joint set in analytical solution

Joint sets	Dip ψ_1 [°]	Dip ψ_2 [°]
1	60	30
2	70	20
3	50	40

Table9. Mechanical characteristics of joint set in analytical solution

Joint sets 1,2,3	Friction Angles φ_1, φ_2 [°]	Cohesion c [MPa]
	20	0
	25	0.1
	30	0.2
	35	0.3
40	0.4	

3.2 Bearing capacity for joint set 1, $\psi_1/\psi_2 = 60/30$

As evident from the equations, the bearing capacity is significantly influenced by the orientation and mechanical properties of the joint set, encompassing both the cohesion and friction angle of the discontinuities. The bearing capacity values for orientations of 60/30 degrees are depicted in figure 19.

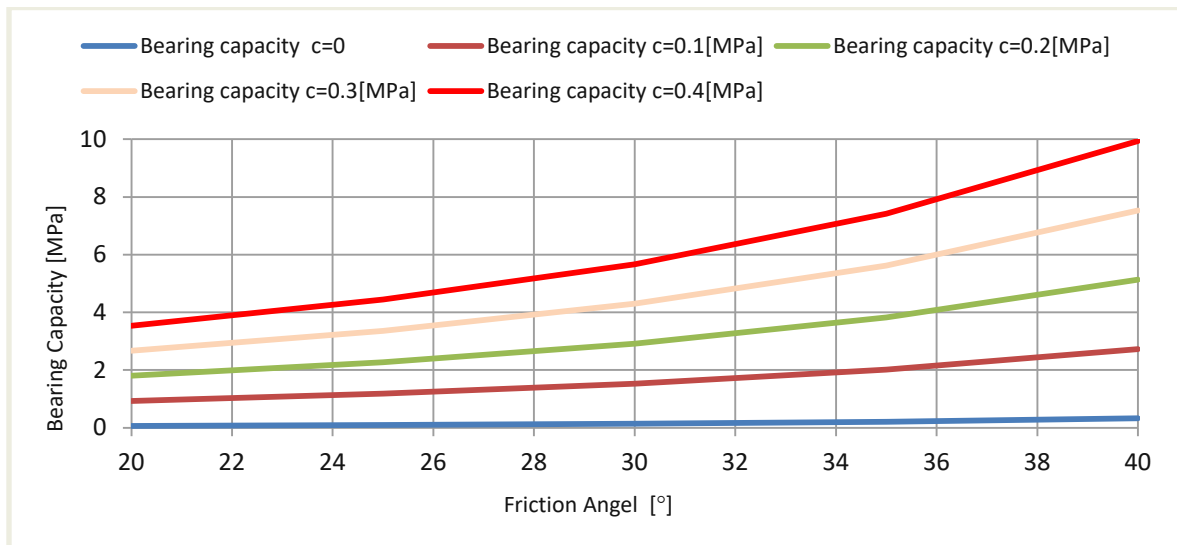


Figure19. Bearing capacity joint sets 1 according to analytical solution

3.3 Bearing capacity for joint set 2, $\psi_1/\psi_2 = 70/20$

By changing the direction of the joint set, as indicated by equations 12.2-12.6, this alteration, unlike changes in cohesion and friction angle, does not have a significant effect on the obtained bearing capacity and the obtained bearing capacities exhibit a lower magnitude compared to the joint set 60/30. This can be observed in figures 20.

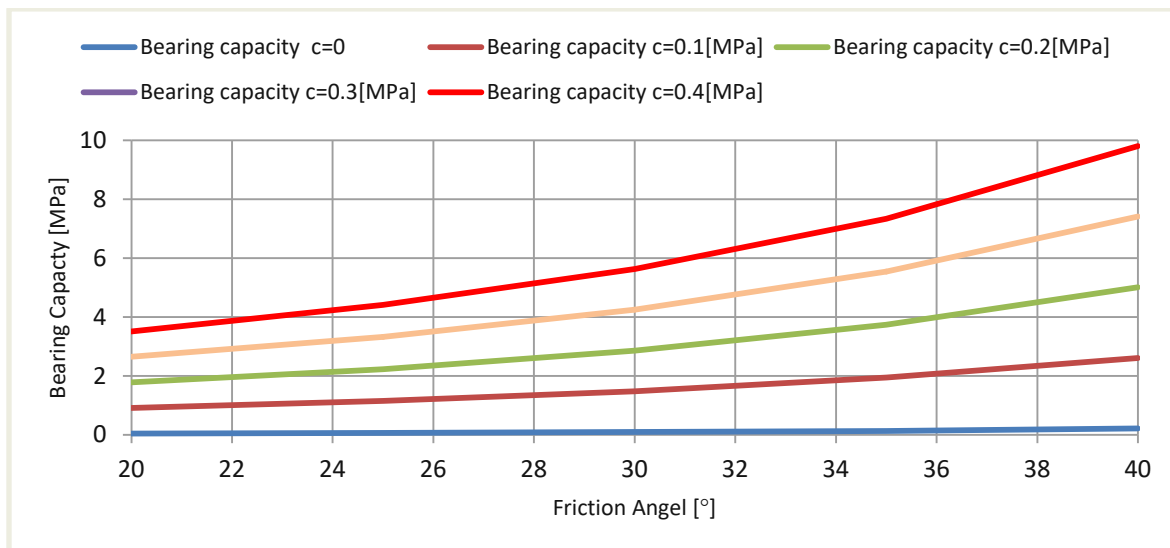


Figure 20. Bearing capacity joint sets 2 according to analytical solution

3.4 Bearing capacity for joint set 3, $\psi_1/\psi_2 = 50/40$

For this orientation, the determination of bearing capacity followed the same methodology as the previous two orientations, as outlined in section 2.4.5. This process is depicted in figure 21. Notably, the highest bearing capacity is observed for the 50/40 orientation, followed by 60/30, and finally 70/20, as illustrated in the figures above.

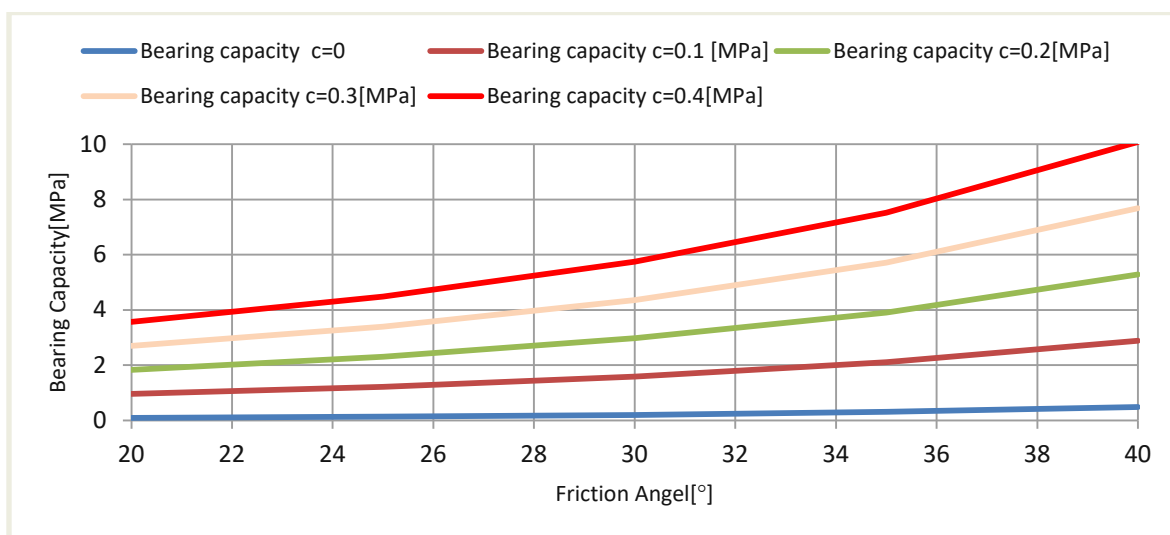


Figure 21. Bearing capacity joint sets 3 according to analytical solution

4 Numerical model

4.1 3DEC

The 3DEC program mainly used in this work is obtained from Itasca Consulting Group Inc. The name "3DEC" stands for 3-Dimensional Distinct Element Code and it works as a numerical program based on the Discrete Element Method (DEM) that is used for discontinuous modeling. Distinct element method can usually easily observe large deformation in joints and also identify all new contacts between blocks due to relative block movement. Through 3DEC, it is possible to model any number of joint sets with different orientations and determined their characteristics.

Blocks can be described both as rigid, having 6 degrees of freedom (3 translational, 3 rotational) and bounded by planar and polygonal surfaces, and as deformable blocks that they are divided into tetrahedral, each of which has 3 degrees of translational freedom (based on Itasca 2007). If the displacements occurring in the model are largely caused by movements in the contact surfaces, the use of rigid bodies is recommended. If there is a lot of deformation in the blocks, the use of deformable bodies is recommended, we attribute the material properties to the bodies, in which case elastic and plastic deformations are possible. To make these changes in blocks, we need to discretize them.

This program discretizes blocks by entering the average tetrahedron edge length into tetrahedron regions. The fineness of the zoning improves the accuracy of deformations, but the calculation time also increases significantly.

4.2 Modeling

Several basic rules must be followed to obtain meaningful results from a numerical model. These rules include the size of the model, the fineness of the areas, the storage conditions, and the material models that the calculation is based on. [38]

For the dimensions of the model, we chose a rectangular block with a length of 40 [m], a width of 1 [m] and a height of 19 [m] (Figure 22). The decision to adopt a one meter width was influenced by our project's goal of studying wedge failure. This selection is in harmony with the foundation's thickness of 1 meter, allowing us to pursue our objective with an appropriately slender model. A foundation of dimensions 2 [m] by 1 [m] is located at point [14, 0, 19] on the block.

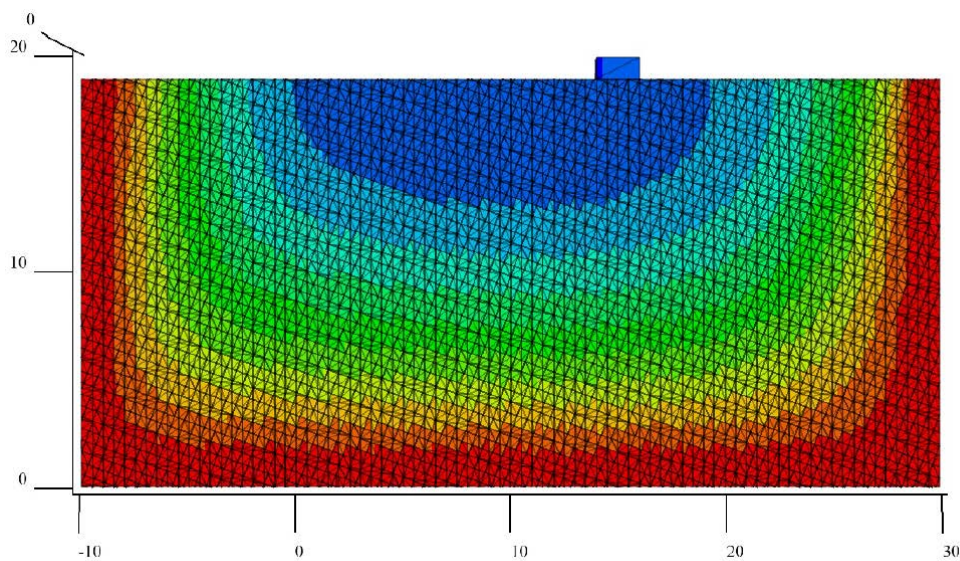


Figure 22. Representation of the model for three-dimensional examinations in 3DEC

The important point in choosing the dimensions of the model is to prevent the displacement and velocity vectors from reaching the boundaries of the model. This issue is clearly evident in the figures 23 and 24.

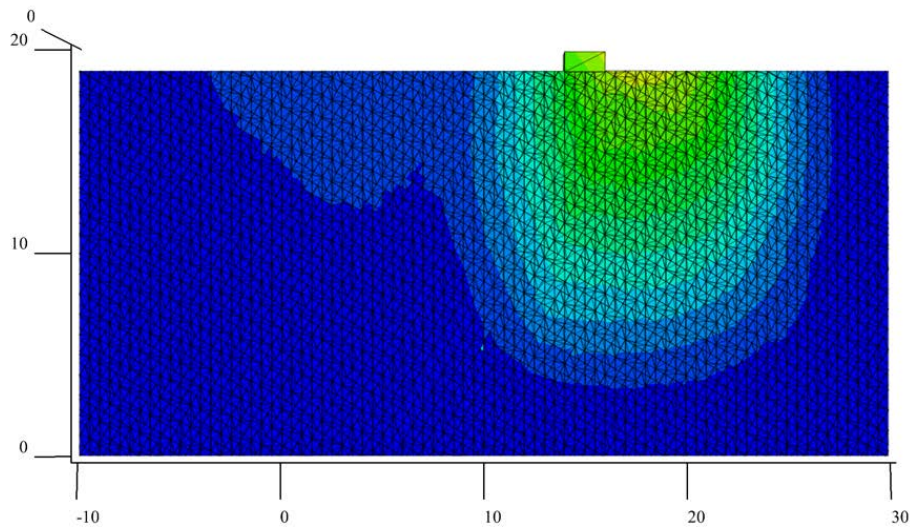


Figure23. The appropriateness of the model dimensions under consideration of the block velocity magnitude does not extend to the boundaries

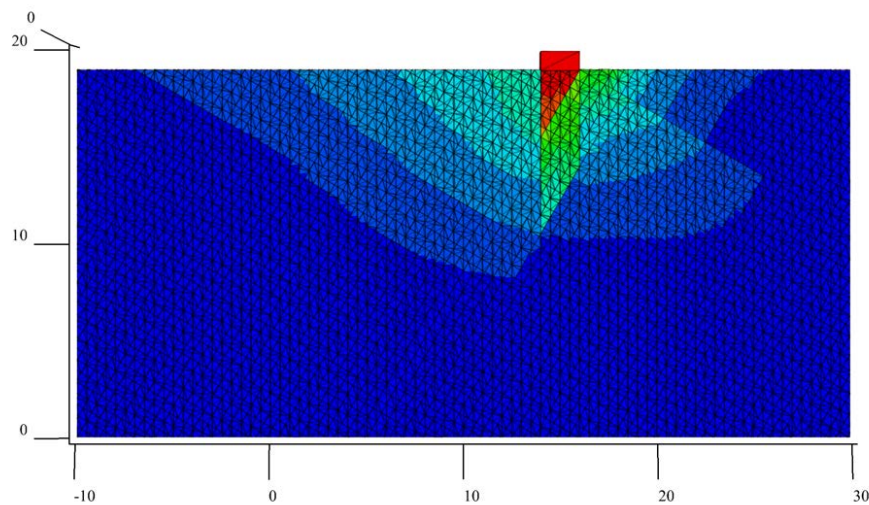


Figure24. The appropriateness of the model dimensions under consideration of the block displacement magnitude does not extend to the boundaries

And as boundary conditions at the beginning [-10 to -9] and at the end [29 to 30] of the model in X direction. Also, at the beginning of the model in the Z direction [0 to 1], all the blocks are fixed in this specified range same as figure 25. Each loading step goes through 10,000 cycles aligned to an estimated limit equilibrium that is achieved in a practical computational time

frame. This numerical value is determined experimentally and ensures the maintenance of a stable state

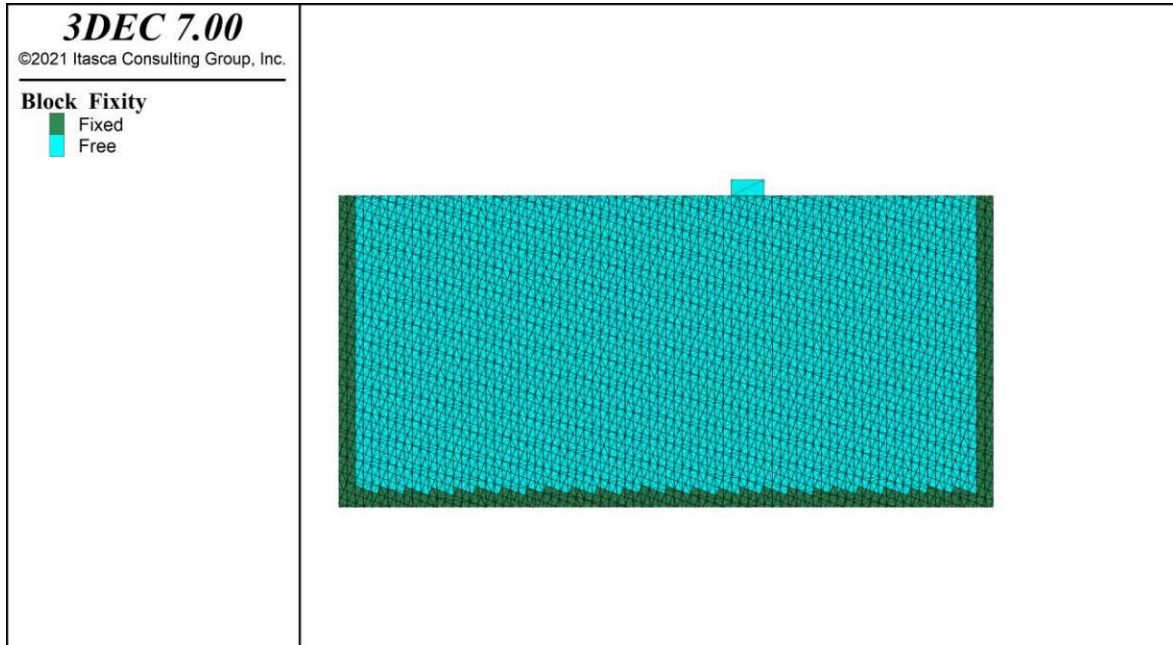


Figure25. Boundary condition in numerical model

4.2.1 Model with 2 joint set

During the initial phase of the numerical approach, a numerical model was constructed using 3DEC software, following the conditions outlined in section 3.1. Specifically, the model featured two joint sets of discontinuities oriented perpendicularly at angles of $\psi_1 = 60$ and $\psi_2 = 30$ degrees, shear stiffness 1[GPa] and normal stiffness 5[GPa] for both of two set with varied friction angles and cohesion values as detailed in the table below and at a distance of 300 [mm] from each other.

For this purpose, to determine the bearing capacity, we considered a rectangular foundation with dimensions of 1[m]*2[m] on the rock mass with a density of 0.027[MN/m³], which contains two sets of orthogonal discontinuities. The mechanical characteristics of the joints are identical, and their corresponding values are provided in the table 10 below. To enhance our comprehension of the influence of the joints orientation, friction angle, dilation angle and cohesion on the foundation's bearing capacity, we have examined three distinct discontinuity orientation states. Additionally, various values for friction angles, dilation angle and cohesion and have been taken into account, as indicated in the table 11 below. We constructed our models by assuming uniform values for both the dilation angle and the friction angle.

Table10. The orientation of the joint set in DEM model with 2 joint set

Joint sets	Dip ψ_1 [°]	Dip ψ_2 [°]
1	60	30

Table11. Mechanical characteristics of joint set in DEM model with 2 joint set

Joint sets 1,2	Friction Angles φ_1, φ_2 [°]	Dilation Angel [°]	Cohesion c [MPa]
	20	20	0
25	25	0.1	
30	30	0.2	
35	35	0.3	
40	40	0.4	

4.2.1.1 Failure model with 2 joint sets

The foundation's bearing capacity was assessed through the consideration of failure modes arising from failures along the discontinuities or across the material. Due to the direction of load application and the angle of joint group one, the main vertical settlement has occurred along this joint.

In order to detect the failure in our model, we considered the criteria of the formation of the failure wedge, displacement magnitude, as well as the velocity magnitude.

In the model featuring two sets of joints, the primary settlement and displacement predominantly manifest in the horizontal direction. This phenomenon is ascribed to the sliding of plates within the joint group, particularly in close proximity to the vertical direction. The observed behavior is a consequence of applied stresses and sliding along the seams. It is noteworthy that, in contrast to the analytical solution, the determination of wedge failure is not conclusive in this context.

As evident from Figure 26, the failure mechanism initiates following significant displacements along the discontinuities. The failure pattern is characterized by a combination of failures along these discontinuities or within the material itself. Our primary criterion is the magnitude of displacement, which directly impacts serviceability.

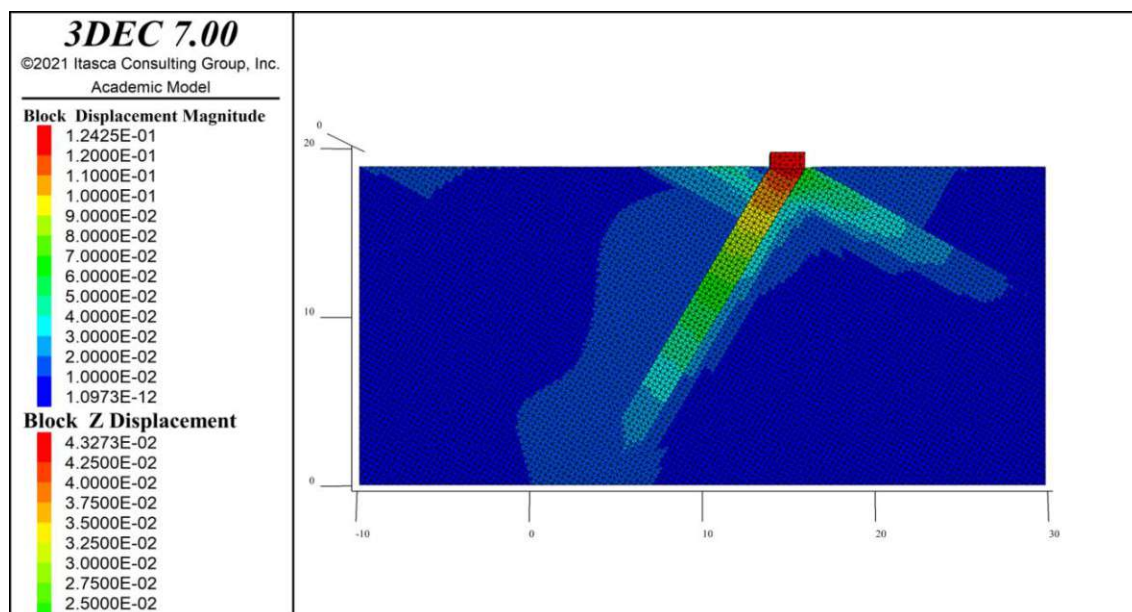


Figure 26. Model failure under Block displacement [m] with a 3 [MPa] load, with a cohesion of 0.2 [MPa] and a friction angle of 20 [°], Numerical model (DEM) with 2-joint set

4.2.2 Model with 3 joint set

As evident from Figure 11, the failure mechanism involves wedge-shaped sliding along the joint, that horizontal stress σ_{3A} playing a crucial role, its presence contingent on the vertical joint. Consequently, a new model was constructed by introducing this vertical joint as the third joint set, and the bearing load capacities for this model were determined. Like the model with two types of joints, the rock density is [0.027 MN/m³] and shear stiffness 1 [GPa] and normal stiffness 5 [GPa] for all three set.

The distance between all three sets of joints was set at 500 [mm] and three different orientations of the joint sets were investigated and the orientations are presented in the table 12 provided below.

Table12. The orientation of the joint set in DEM model with 3 joint set

Joint sets	Joint-set with Dip ψ_1 [°]	Joint-set with Dip ψ_2 [°]	Joint-set with Dip ψ_3 [°]
1	60	30	90
2	70	20	90
3	50	40	90

In order to determine the bearing capacity using three sets of joints, a constant friction angle of 20 degrees was maintained, while the dilation angle was set equal to the friction angle at 20 degrees. The cohesion of the joint sets varied within a specific range as detailed in Table 13 below. We chose a friction angle of 20 degrees because it yielded the highest agreement between the results obtained from the model and the analytical solution. In other cases, the differences between the results exhibited a significant increase.

Table13. Mechanical characteristics of joint set in DEM model with 3 joint set

Joint sets 1,2,3	Friction Angles $\varphi_1, \varphi_2, \varphi_3, [^\circ]$	Dilation Angel $[^\circ]$	Cohesion c [MPa]	Shear stiffness [GPa]	Normal stiffness [GPa]
	20	20	0	1	5
			0.1		
			0.2		
			0.3		
			0.4		

4.2.2.1 Failure model with 3 joint sets

A significant aspect of the failure criterion in the model with three types of joints was the occurrence of wedge failure. Before the formation of the wedge failure, the values of magnitude displacement and velocity were low, however, following the wedge failure, these values increased significantly. As evident from the fracture patterns figure 28-33. The orientation of the joints plays a crucial role in the formation of these wedges and the criteria for failure (magnitude of displacement and velocity). The highest magnitudes of displacement and velocity are observed in the 60/30 orientations (Figure30-31).

Unlike the numerical model with two sets of joints, where the absence of wedge failure is crucial, our criterion for failure is the magnitude of displacement and its impact on serviceability (Figure 26).The behavior of the model with three joint sets aligns with the analytical solution framework, clearly illustrating the well-known failure mechanism described.

5 Result

5.1 Bearing capacity numerical model with 2 joint set

As elucidated in section 4.2.1, the failure mechanism in the model featuring two sets of joints deviates from the formation of a wedge failure. Instead, failure manifests under high displacement, followed by sliding along the joint set, as distinctly illustrated in Figure 26.

In the table 14-18, you can observe the permissible bearing capacity values for various cohesion levels and different friction angel modes.

Table14. Bearing capacity of foundation for the DEM model with 2 joint set under cohesion 0

Cohesion $c=0$	
friction angles φ_1 and φ_2 [°]	Bearing Capacity q_a [MPa]
20	1
25	1.3
30	2
35	3.3
40	4.5

Table15. Bearing capacity of foundation for the DEM model with 2 joint set under cohesion 0.1 [MPa]

Cohesion $c=0.1$ [MPa]	
friction angles φ_1 and φ_2 [°]	Bearing Capacity q_a [MPa]
20	1.8
25	2.5
30	3.8
35	5.5
40	6.6

Table16. Bearing capacity of foundation for the DEM model with 2 joint set under cohesion 0.2 [MPa]

Cohesion $c=0.2$ [MPa]	
friction angles φ_1 and φ_2 [°]	Bearing Capacity q_a [MPa]
20	2.6
25	3.4
30	4.9
35	6.4
40	7.6

Table17. Bearing capacity of foundation for the DEM model with 2 joint set under cohesion 0.3 [MPa]

Cohesion $c=0.3$ [MPa]	
friction angles φ_1 and φ_2 [°]	Bearing Capacity q_a [MPa]
20	3.2
25	4.2
30	5.8
35	7.3
40	8.5

Table18. Bearing capacity of foundation for the DEM model with 2 joint set under cohesion 0.4 [MPa]

Cohesion $c=0.4$ [MPa]	
friction angles φ_1 and φ_2 [°]	Bearing Capacity q_a [MPa]
20	4.1
25	5,6
30	7.1
35	8.6
40	10.7

The figure 28 is clear. Firstly, the trend of the diagram is linear, similar to the analytical solution diagrams. Secondly, the values of the bearing capacity exhibit a significant increase compared to analytical method. It is noteworthy that the analytical equation does not account for the effect of the distance between the joint sets and mechanical properties such as normal and shear stiffness on bearing capacity, indeed, it is evident that as the distance between joint sets increases, the dimensions of our blocks also increase, resulting in a higher bearing capacity. As mentioned earlier, we considered a distance between the joint sets of 300 [mm], leading to the obtained results.

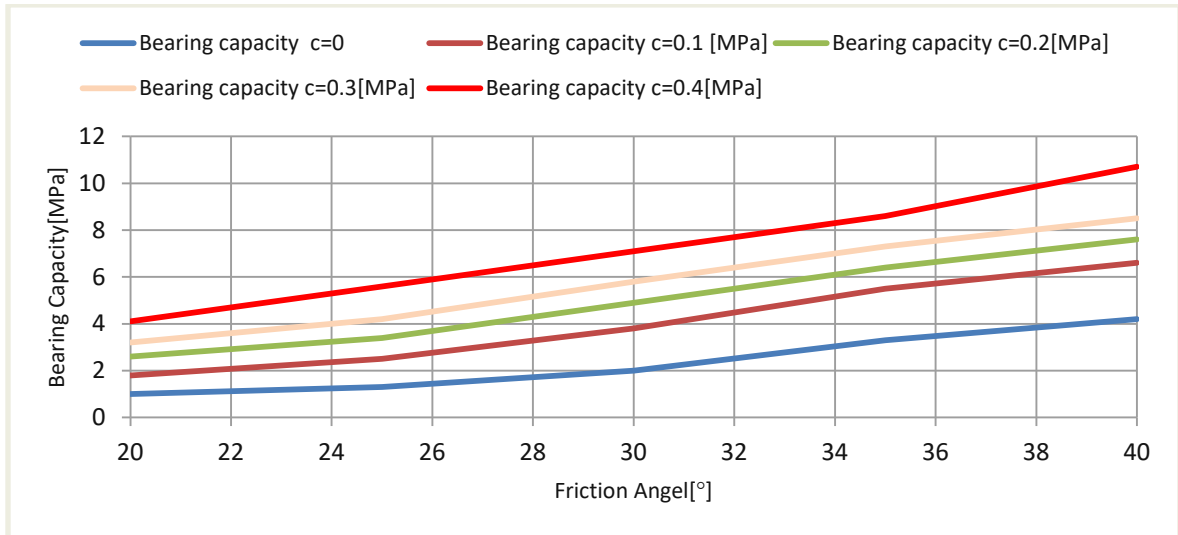


Figure27. Bearing capacity for DEM model with 2joint sets and dipping $\psi_1 = 60 [^\circ]$ and $\psi_2 = 30 [^\circ]$ and Spacing 300 [mm]

5.2 Bearing capacity numerical model with 3 joint set

In the improved model featuring three joint sets, the pronounced proximity of both the failure mechanism and bearing capacity to the analytical solution presented by Ladanyi and Roy (1971) is readily apparent.

5.2.1 Wedge failure for joint sets 1, $\psi_1/\psi_2 = 60/30$

The highest load-bearing capacities obtained from the DEM (3DEC) for this situation were observed in the direction of this joint set, as illustrated in the table 19.

Table19. Bearing capacity of foundation under wedge failure for joint sets 1 with friction angel 20 [°]

Cohesion c [MPa]	Bearing Capacity q_a [MPa]
0	0.5
0.1	0.9
0.2	1.6
0.3	2.2
0.4	2.7

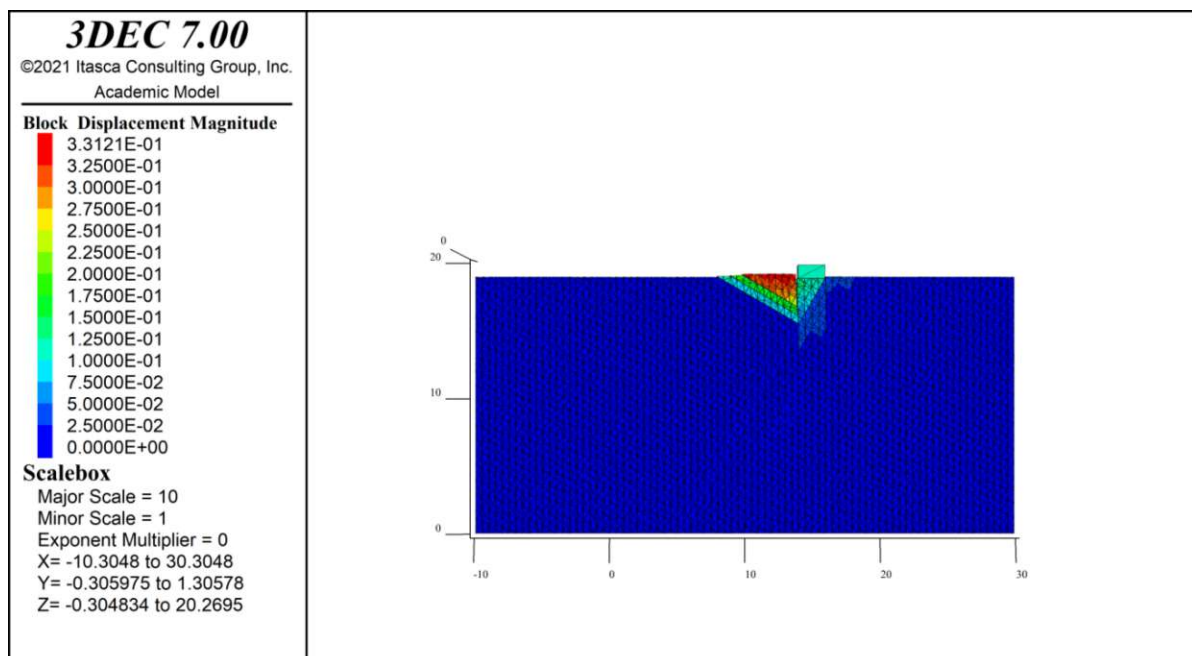


Figure28. Wedge failure for joint sets 1 under Block displacement magnitude [m] for 2.3 [MPa] load and cohesion 0.3 [MPa], Friction angel 20 [°]

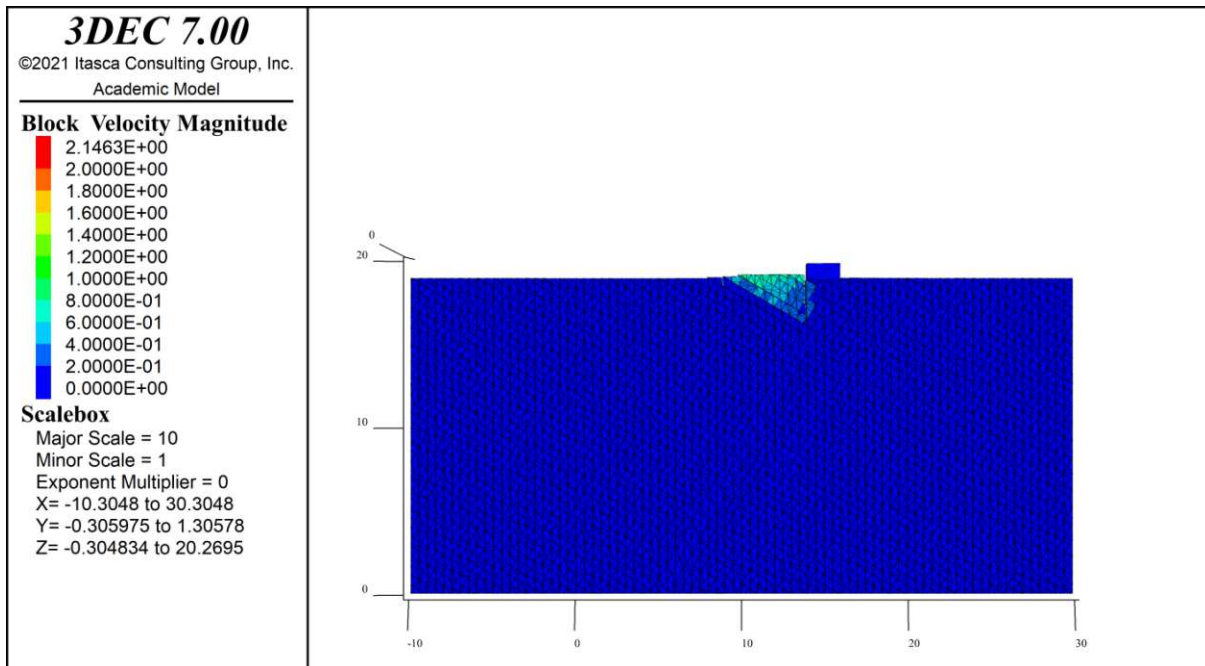


Figure29. Wedge failure for joint sets 1 under Block velocity magnitude [m/s] for 2.3 [MPa] load and cohesion 0.3 [MPa], Friction angel 20 [°]

As evident from the failure figure 29 and 30, the most prominent failure wedge occurs in this case, and the failure mechanism clearly indicates the outward movement of the passive wedge formed under the foundation.

5.2.2 Wedge failure for joint sets 2, $\psi_1/\psi_2 = 70/20$

Following joint set 1, the highest load capacity is attributed to joint set in state 2, and the corresponding values of this load capacity are provided in the table 20.

Table20. Bearing capacity of foundation under wedge failure for joint sets 2 with friction angel 20 [°]

Cohesion c [MPa]	Bearing Capacity q_a [MPa]
0	0.6
0.1	0.9
0.2	1.3
0.3	1.8
0.4	2.2

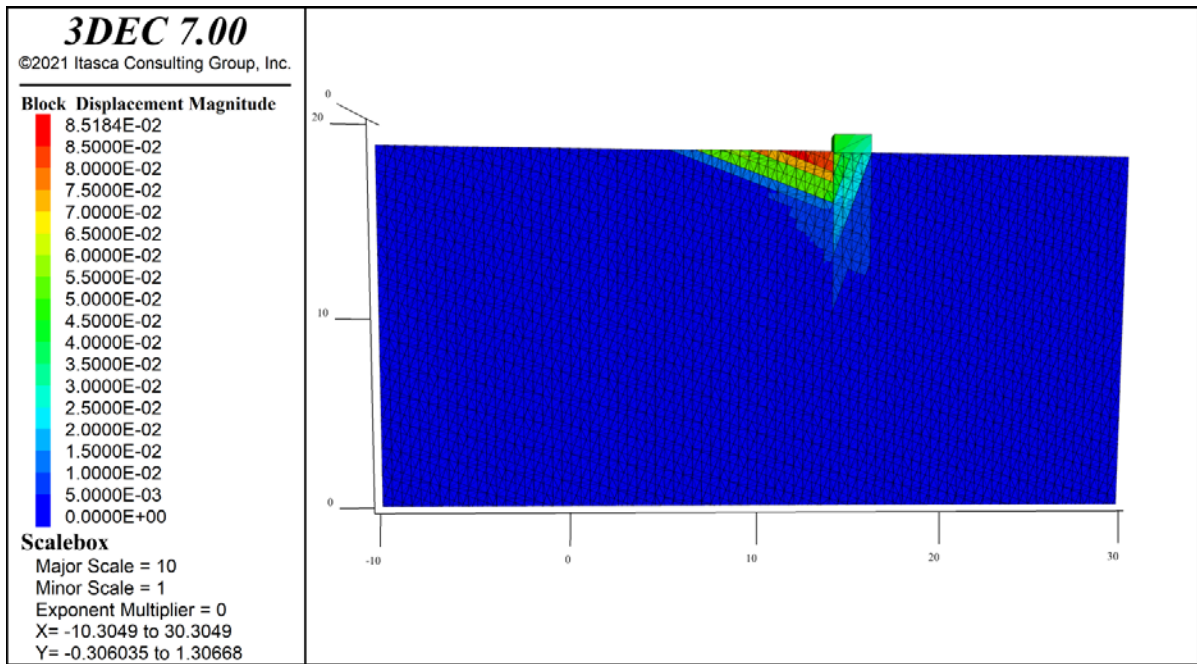


Figure30. Wedge failure joint sets 2 under Block displacement magnitude [m] for 1 [MPa] load and cohesion 0.1 [MPa], Friction angel 20 [°]

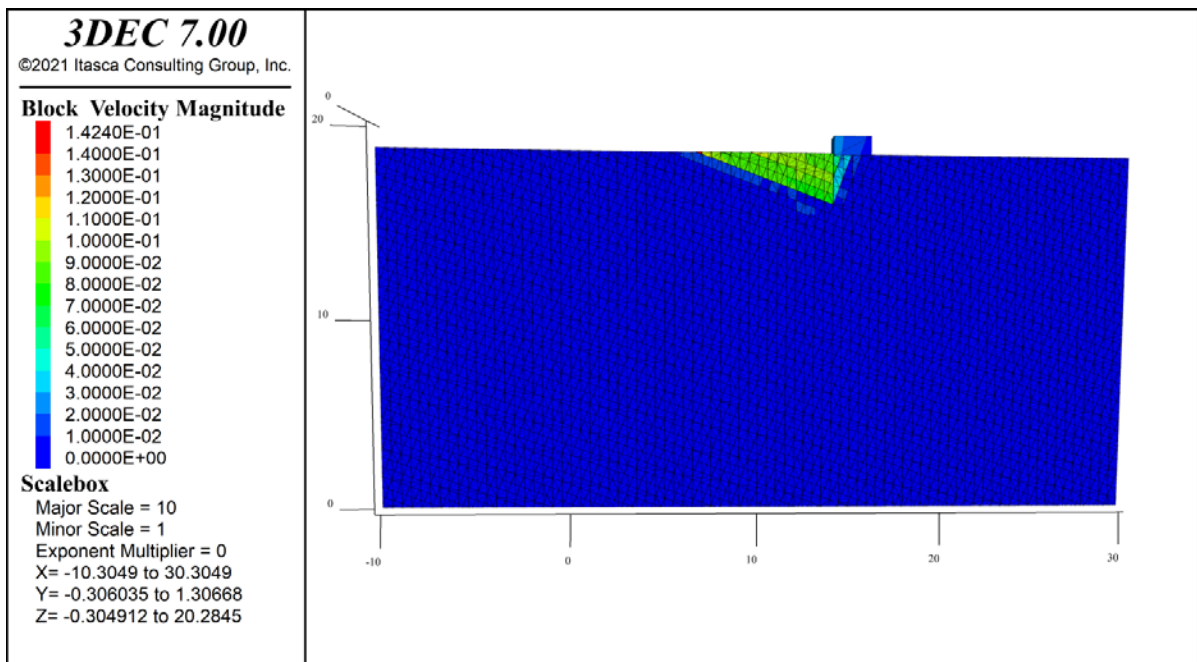


Figure31. Wedge failure joint sets 2 under Block velocity magnitude [m/s] for 1 [MPa] load and cohesion 0.1 [MPa], Friction angel 20 [°]

The failure figure 31 and 32 clearly indicates that the failure wedge is formed on the left side of the foundation, similar to the joint set 1. However, the dimensions of the formed wedges are smaller than those observed in the joint set 1.

5.2.3 Wedge failure for joint sets 3, $\psi_1/\psi_2 = 50/40$

The lowest bearing capacity among these three states of joint set belongs to this state, whose values can be seen in the table 21 below.

Table21. Bearing capacity of foundation under wedge failure for joint sets 3 with friction angel 20 [°]

Cohesion c [MPa]	Bearing Capacity q_a [Mpa]
0	0.6
0.1	0.8
0.2	1.1
0.3	1.5
0.4	2

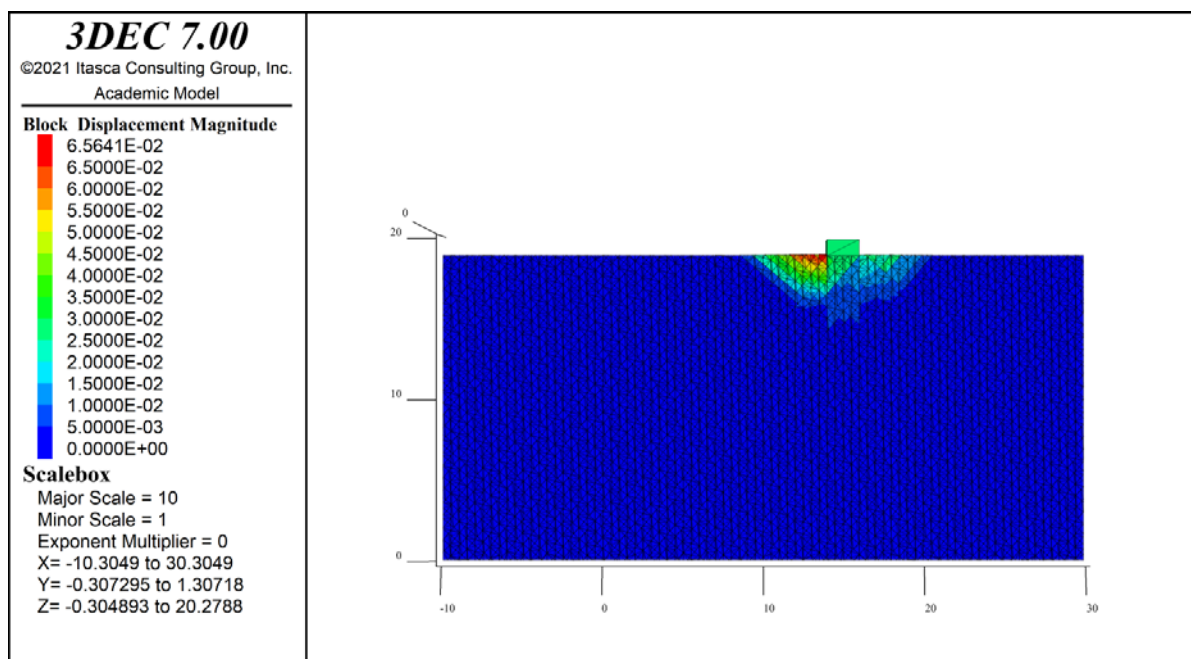


Figure32. Wedge failure joint sets 3 under Block displacement magnitude [m] for 0.9 [MPa] load and cohesion 0.1 [MPa], Friction angel 20 [°]

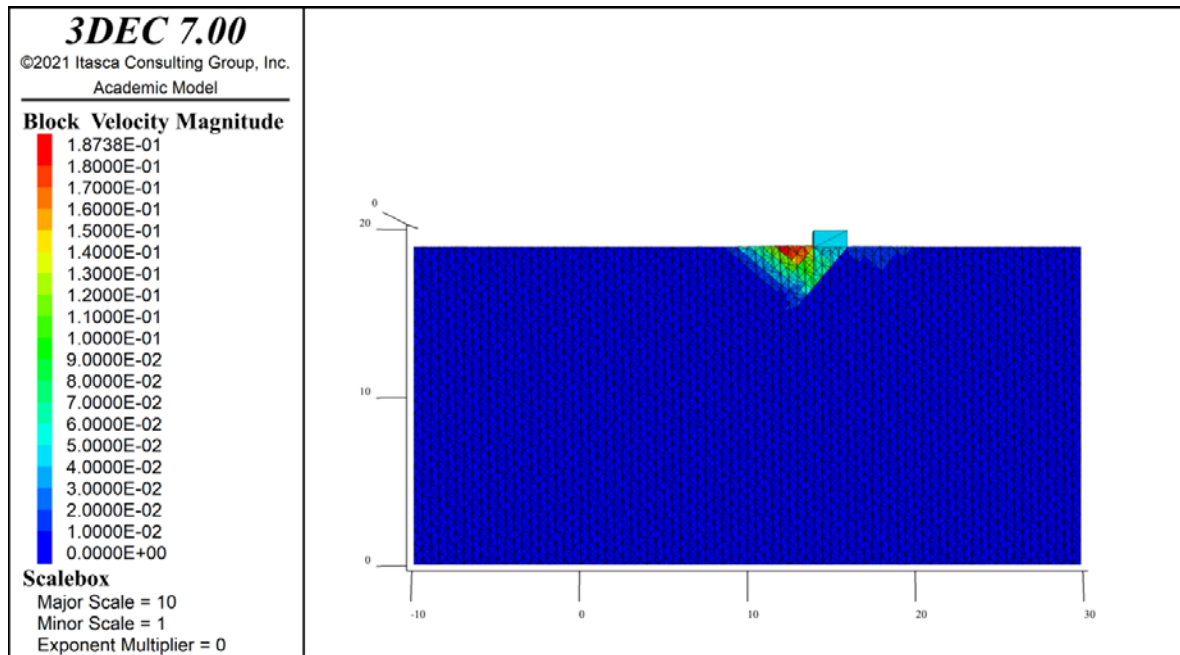


Figure33. Wedge failure joint sets 3 under Block velocity magnitude [m/s] for 0.9 [MPa] load and cohesion 0.3 [MPa], Friction angel 20 [°]

In this case, a noteworthy observation emerges as the location of the fractured wedge differs from the previous two instances. In certain state, it is situated on both sides of the foundation (Figure33 and 34), while in others state, it is specifically on the right side of the foundation. Furthermore, its size, as depicted in the accompanying figures, is comparatively smaller than in the preceding two cases.

5.2.4 The impact of joint set orientation on bearing capacity

It is well known from the results in tables 19, 20 and 21 that the orientation of the joints has a significant effect on the bearing capacity, and it is clear from the figure 35 that the highest bearing capacity is 30/60 and the lowest is 40/50 and with the increase of cohesion value from 0.1 [MPa], the difference between them increases. The concept can be well understood by considering the stress distribution in jointed rocks, as explained in section 2.4.4, and its effect on the formation of a fracture wedge.

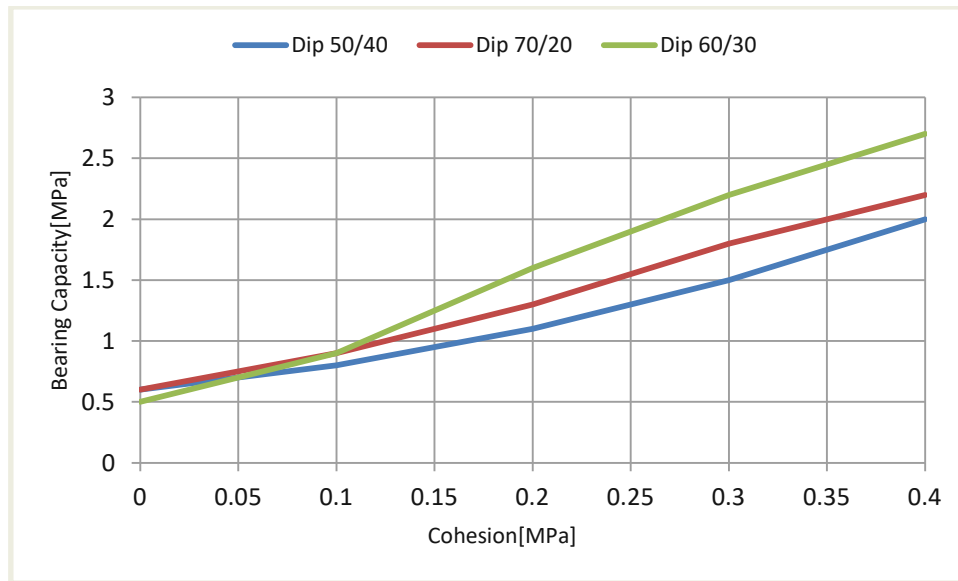


Figure 34. The impact of joint set orientation on bearing capacity

5.3 New approach in reverse calculations between DEM and analytical method

As explained in section 2.4, one of the ways to find the bearing capacity for rocks with two types of joints set is to use the diagrams in the standard. In this section, first, with the values of cohesion "c" and friction angles of discontinuity sets " φ " and the value of the bearing capacity q_a of the foundation obtained from the software 3DEC (DEM), according to the existing formula of analytical equation, we calculate the amount of the minimum principal stress σ_{3A} that acts horizontally on the active wedge A.

$$\sigma_{3A} = \frac{[q_a - (c_1 / \tan \psi_1)] (N_{\phi 1} - 1)}{N_{\phi 1}} \quad (5.1)$$

$$N_{\phi 1} = \tan^2 \left(45 + \frac{\varphi_1}{2} \right) \quad (5.2)$$

The illustration in the standard explicitly indicates the foundation's bearing capacity on rock, considering the uniaxial compressive strength of intact rock and the joint distances. Figure 17 in section 2.8 highlights that the uniaxial compressive strength of the jointed rock mass is approximately 10% of that of intact rock. As a result, we multiply minimum principal stress σ_{3A} from the above formula by 10 times and consider it as the stress of intact rock and

according to the uniaxial compressive strength and the distance between the joints which is 500 [mm], we read the bearing capacity from the chart, which is bearing capacity is very close to the capacity obtained from the 3DEC (DEM). For joint sets 1 with orientations $\psi_1=60$ degrees and $\psi_2=30$ degrees, these values are available in Table 22.

Table 22. Minimum principal stress σ_{3A} through inverse calculations involving Discrete Element Method (DEM) and analytical approaches for first joint set

Cohesion c [MPa]	Bearing Capacity q_a [MPa]	σ_{3A} [MPa]	$10*\sigma_{3A}$
0	0.5	0.24	2.4
0.1	0.9	0.41	4.1
0.2	1.6	0.72	7.2
0.3	2.2	0.99	9.9
0.4	2.7	1.15	11.5

Presently, with stress $10*\sigma_{3A}$ measurements and the joint set distance 500 [mm] in hand, as depicted in the figure 36, the bearing capacity can be readily determined by reading from the diagram.

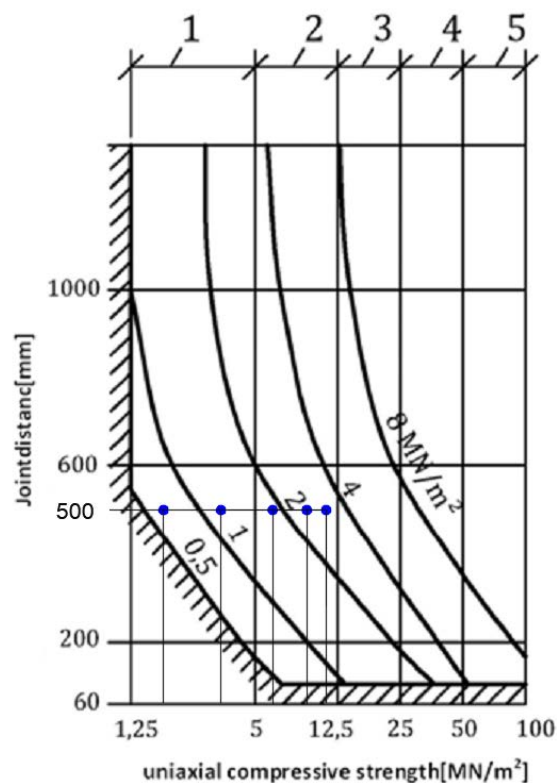


Figure35. Bearing capacity through inverse calculations involving Discrete Element Method (DEM) and analytical approaches for first joint set $\psi_1 = 60 [^\circ]$ and $\psi_2 = 30 [^\circ]$

The calculated values for the joint sets with orientation $\psi_1 = 70$ degree and $\psi_2 = 20$ degree are in the table 23 and the results are depicted in Figure 37.

Table23. Minimum principal stress σ_{3A} through inverse calculations involving Discrete Element Method (DEM) and analytical approaches for the second joint set

Cohesion c [MPa]	Bearing Capacity q_a [MPa]	σ_{3A} [MPa]	$10 * \sigma_{3A}$
0	0.6	0.29	2.9
0.1	0.9	0.42	4.2
0.2	1.3	0.6	6
0.3	1.8	0.83	8.3
0.4	2.2	1	10

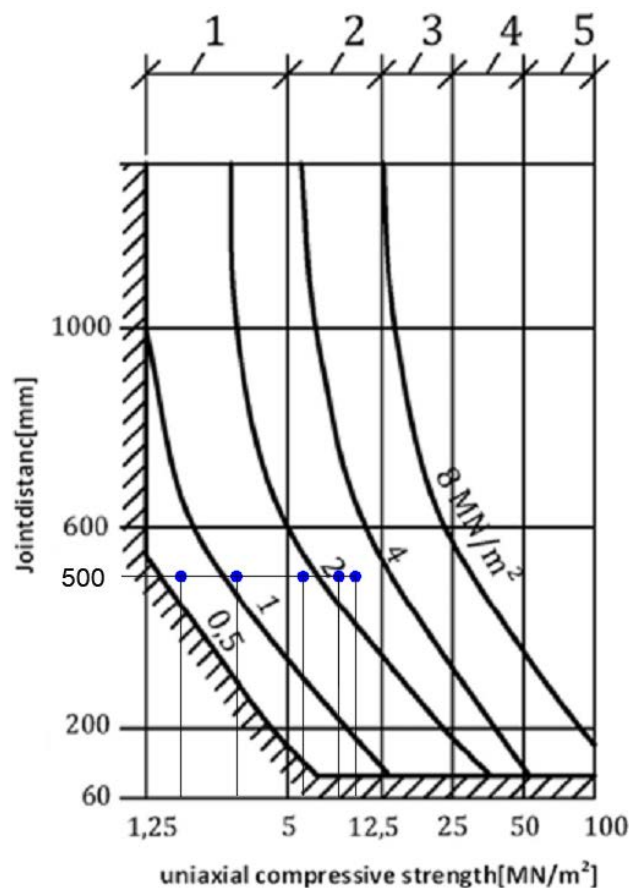


Figure36. Bearing capacity through inverse calculations involving Discrete Element Method (DEM) and analytical approaches for two joint set $\psi_1 = 70 [^\circ]$ and $\psi_2 = 20 [^\circ]$

And also for the joint sets with orientation $\psi_1=50$ degree and $\psi_2=40$ degree these values are available in the table 24 and the results are depicted in Figure 38.

Table24. Minimum principal stress σ_{3A} through inverse calculations involving Discrete Element Method (DEM) and analytical approaches for the third joint set

Cohesion c [MPa]	Bearing Capacity q_a [MPa]	σ_{3A} [MPa]	$10*\sigma_{3A}$
0	0.6	0.3	3
0.1	0.8	0.35	3.5
0.2	1.1	0.45	4.5
0.3	1.5	0.61	6.1
0.4	2	0.8	8

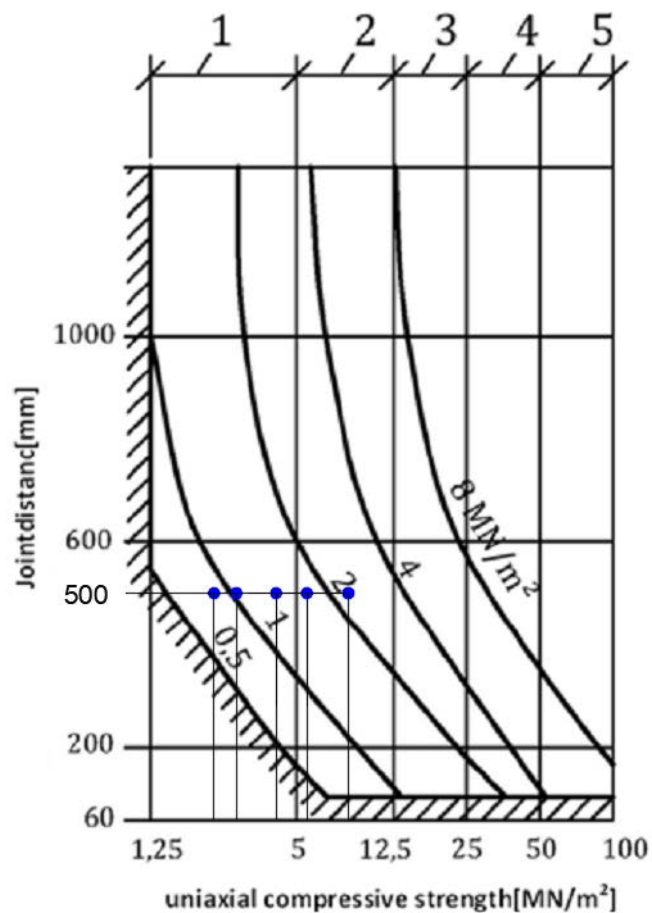


Figure37. Bearing capacity through inverse calculations involving Discrete Element Method (DEM) and analytical approaches for third joint set $\psi_1 = 50$ [°] and $\psi_2 = 40$ [°]

6 Interpretation and comparison of the results

6.1 Comparison of the results of the analytical methods with numerical model (DEM) with 2 joint set

In Section 4-2-1, it was revealed that the bearing capacities obtained from the numerical model, featuring two sets of perpendicular joints with dipping angles $\psi_1 = 60$ and $\psi_2 = 30$ degrees, demonstrate a difference when compared to the results derived from analytical solutions. This contrast arises because the wedge failure mechanism in the numerical model, established using the Discrete Element Method (DEM), occurs after extensive displacement and settlement in the blocks and as it is well known, by reducing the spacing between the joints, the size of the blocks becomes smaller and the bearing capacity obtained in this case is smaller and it is close to the bearing capacity obtained from analytical solution.

However, due to the abundance of contact surfaces between the blocks in the model with small spacing, the software requires an extensive duration, approximately two days, to conduct a thorough analysis of the model. Therefore, the bearing capacities obtained for the model with two joint sets with 300[mm] show higher values than the analytical solution and this fact is illustrated in Figure 39.

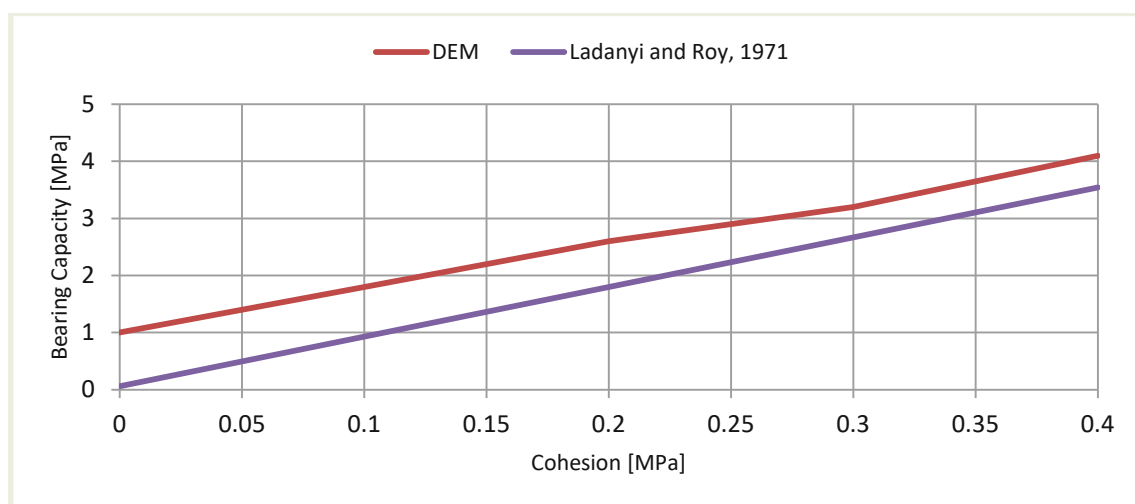


Figure38. The comparison the bearing capacity of the numerical model, which incorporates two varieties of joints, a spacing of 300 [mm], and dip direction of $\psi_1 = 60$ [°] and $\psi_2 = 30$ [°], with the Analytical relationships proposed.

6.2 Comparison of the results of the analytical methods with numerical model (DEM) with 3 joint set

6.2.1 Joints set 1, $\psi_1/\psi_2 = 60/30$

Based on the results obtained from the numerical model that includes three sets of joints, it can be inferred that the bearing capacity derived from the model, featuring a friction angle of 20 degrees and a joint spacing of 500 [mm], closely corresponds to the bearing capacity obtained through analytical methods refer to Figure 39 . Moreover, the wedge failure mechanism observed in this model exhibits similarities to Figure 11 and aligns with the approach described by Ladanyi and Roy.

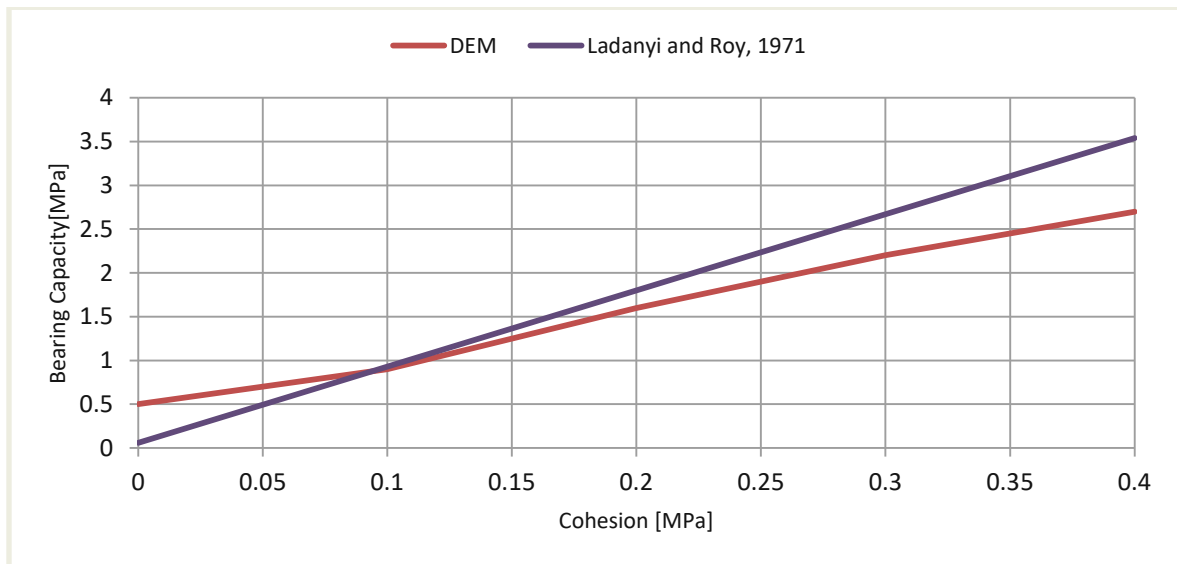


Figure39. The comparison the bearing capacity of the numerical model, which incorporates three varieties of joints with friction angel 20 [°], spacing of 500 [mm], and dip direction of $\psi_1 = 60$ [°] and $\psi_2= 30$ [°] and $\psi_3= 90$ [°], with the analytical relationships proposed.

6.2.2 Joints set 2, $\psi_1/\psi_2 = 70/20$

The comparison of the bearing capacity in this orientation is illustrated in the figure 40 below.

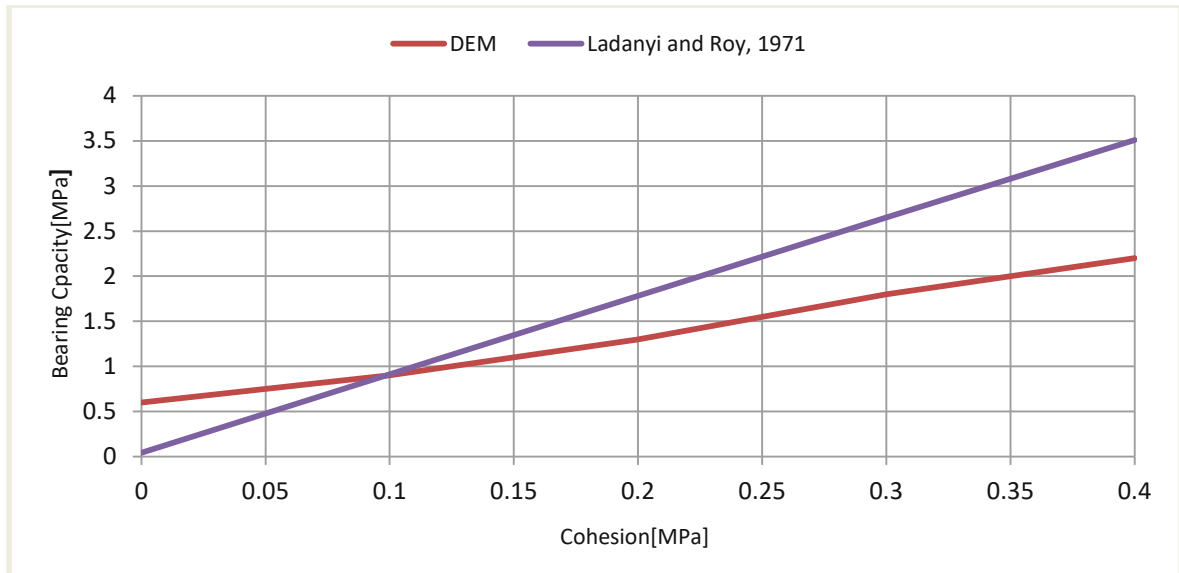


Figure40. The comparison the bearing capacity of the numerical model, which incorporates three varieties of joints with friction angel 20 [°], spacing of 500 [mm], and dip direction of $\psi_1=70$ [°] and $\psi_2=20$ [°] and $\psi_3=90$ [°], with the analytical relationships.

6.2.3 Joints set 3, $\psi_1/\psi_2 = 50/40$

The results of the bearing capacity comparison for this case, similar to the two cases mentioned above, are depicted in the figure below.

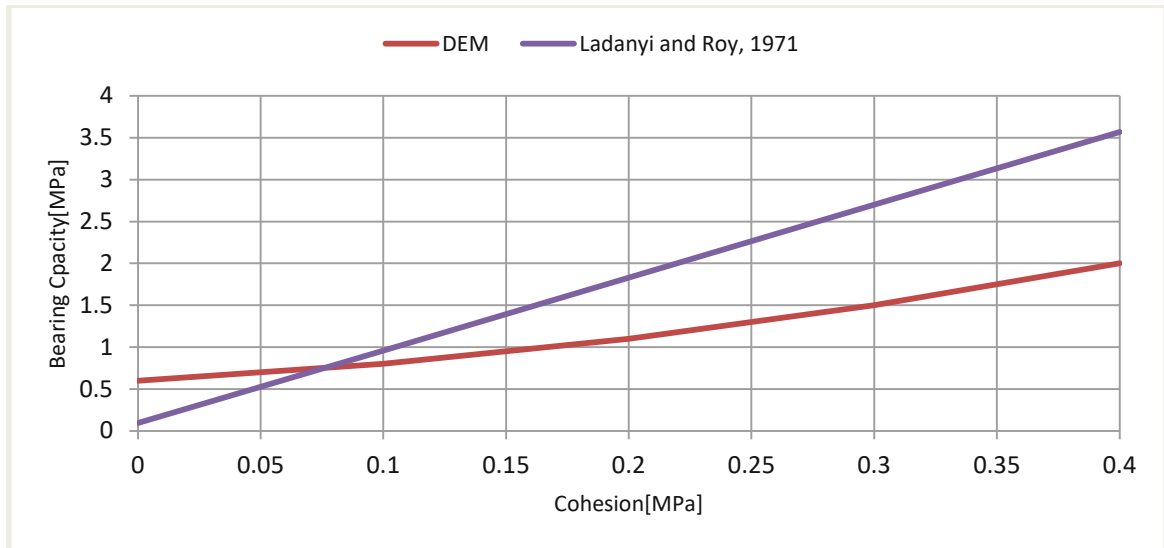


Figure 41. The comparison the bearing capacity of the numerical model, which incorporates three varieties of joints with friction angle 20° , spacing of 500 [mm], and dip direction of $\psi_1 = 50^\circ$ and $\psi_2 = 40^\circ$ and $\psi_3 = 90^\circ$, with the analytical relationships proposed.

A notable observation across all three graphs is that, at cohesion of 0.1 [MPa], the results from the numerical model (DEM) align with the analytical relations. However, for cohesion values below this threshold, the bearing capacity derived from the numerical model surpasses that of the analytical relations. Conversely, for cohesion values exceeding 0.1 [MPa], the trend is reversed, with the bearing capacity obtained from the numerical model (DEM) falling below that of the analytical relations (Figure 41).

Comparable results were calculated by Preh [40] using a dilation angle equal to half the friction angle.

7 SUMMARY

The present study aimed to investigate the influence of the orientation of joint set in foundations on fractured rock. A predefined failure mechanism, such as the sliding of a wedge on an interface, was analyzed in detail according to the ÖNORMEN B 1997-1-2 standards. Particular attention was given to considering the spatial orientation of interfaces in foundations through three-dimensional calculations.

The calculations were conducted using the following methods:

- The analytical limit equilibrium method by Ladanyi and Roy (1971).
- The computational program 3DEC, which allows for a numerical investigation based on the Discrete Element Method (DEM).

All investigations were carried out following the Mohr-Coulomb failure criterion. The strength parameters, namely cohesion and friction angle of potentially existing interfaces, were reduced compared to intact rock.

The bearing capacities derived from the analytical solution effectively demonstrate the impact of joint friction angle and cohesion on the outcomes. However, these relationships do not comprehensively account for the orientation and spacing of the joints and this observation is clearly evident when examining the graphs depicting the bearing capacities derived from the analytical solution.

To enhance the comprehension of the influence of joint orientation, spacing, and the wedge failure mechanism, a numerical model was constructed using the Discrete Element Method (DEM) with the aid of 3DEC software.

The initial model, constructed based on the assumptions of the analytical solution with two sets of joints perpendicular to each other, exhibits a failure mechanism distinct from sliding wedge rupture (Figure 26). Additionally, it demonstrates a higher bearing capacity compared to numerical methods, as clearly illustrated in the tables 14-18 and figure 39. But the point to consider in this model is the spacing of 300 [mm], by reducing this spacing, results very close to the analytical solution can be obtained, but with a different failure mechanism than wedge failure.

The improvements made to the constructed model, including the incorporation of a third joint set with a vertical orientation and identical mechanical properties as the existing two joint sets, resulted in a modification of the failure mechanism in line with the analytical solution (Figure 28-30-31). Remarkably, the bearing capacity obtained under joint spacing set at 500 [mm] and a friction angle of 20 degrees exhibits substantial agreement with the analytical solution results, particularly for the orientation 60/30, especially when cohesion is less than 0.1 [MPa]. However, this agreement diminishes, and the results become inconsistent with increasing cohesion beyond 0.1 [MPa] (Figure 40).

The figure derived from the failure mechanism clearly illustrates the significant influence of the joint set orientation on the formation of wedge failure, as per the analytical solution. The obtained results indicate that the joint set with an orientation of 60/30 is the most compatible (Figure40). It is noteworthy to observe the seam with the 50/40 direction, where wedge failure occurs on both sides, and it has the smallest size compared to other directions (Figure33).

Indeed, the behavior of rock masses is significantly influenced by the characteristics of joint sets. Numerous studies by various authors have consistently confirmed this observation. The discontinuity system, comprised of joints and fractures, often plays a more crucial role in determining the behavior of the rock mass compared to any other material parameter. [39]

Considering that the bearing capacity in ÖNORMEN B 1997-1-2 standards is based on the analytical solution (Ladanyi and Roy 1971), and as mentioned earlier, these relations do not comprehensively account for the influence of joint set direction and distance, caution and meticulous attention should be exercised when selecting values in accordance with the standard. It is crucial to recognize the limitations of the standard and, if necessary, supplement the analysis with additional considerations to ensure a more accurate representation of the real-world conditions.

8 List of literature

- [1] ICOLD (1993) “Rock Foundations for Dams”. ICOLD, Bulletin 88, Paris.
- [2] Duncan C.Wyllie, (2005) “Foundations on Rock”, This edition published in the Taylor & Francise-Library, pp 43.
- [3] Carter, J.P., and Kulhawy, F.H., 1988 “Analysis and Design of Foundations Socketed into Rock”, Report No.El-5918, Empire State Electric Engineering Research Institute, New York, NY, 158p.
- [4] Tang, J., Liu Y., 2012. Bearing Capacity Calculation of Rock Foundation based on Nonlinear Failure Criterion. IERI Procedia, 1: 110–116.
- [5] Souley, M., Homand, F., 1996. Stability of jointed rock masses evaluated by UDEC with an extended Saeb-Amadei constitutive law. International Journal of Rock Mechanics and Mining Sciences & Geomechanics Abstracts, 33(3): 233–244.
- [6] Hoek E., Brown E. T. (1997) “Practical estimates of rock mass strength” International Journal of Rock Mechanics and Mining Sciences, 34, 8, pp 1165-1186.
- [7] Khani A., Baghbanan A., Hashemolhosseini H. (2013) “Numerical investigation of the effect of fracture intensity on deformability and REV of fractured rock masses” International Journal of Rock Mechanics and Mining Sciences, 63, pp 104-112.
- [8] Min K. -B., Jing, L. (2003) “Numerical determination of the equivalent elastic compliance tensor for fractured rock masses using the distinct element method” International Journal of Rock Mechanics & Mining Sciences, 40, pp 795-816.
- [9] Goodman, R.E. (1980), “Introduction to Rock Mechanics”, Wiley, New York, pp. 305–8.
- [10] Developments in the characterization of complex rock Slope deformation and failure using numerical modelling techniques D. Stead a, E. Eberhardt b, J.S.

-
- [11] Wyllie, D.C., 1999“Foundation on Rock masses, Butter Worth Heineman.
 - [12] Engineering and Design ROCK FOUNDATIONS Department of the Army U.S. Army Corps of Engineers Washington, DC 20314-1000.
 - [13] Ladanyi, B. and Roy, A. (1971). Some aspects of the bearing capacity of rock mass. Proc. 7th Canadian Symp. Rock Mechanics, Edmonton.
 - [14] Hoek, E. and Brown, E. T. (1988) The Hoek-Brown failure criterion - a 1988 update. 15th Canadian Rock Mechanics Symposium, Toronto, Canada.
 - [15] Sowers, G. F. (1970) Introductory Soil Mechanics and Foundations, Macmillan New York, pp. 395-6.Sowers, G. F. (1975) Failures in limestone in humid subtropics. ASCE, 101(GT8), 771-87.
 - [16] International Society for Rock Mechanics (ISRM) (1985) Suggested method for determining point load strength. Int. J. of Rock Mech., 22(2), 53-60.
 - [17] Lambe, T. W. and Whitman, R. V. (1969) Soil Mechanics. John Wiley, New York.
 - [18] The Significance of In Situ Tests on Large Rock Specimens Z. T. BIENIAWSKI W. L. VAN HEERDEN.
 - [19] Price, N.J, and J.W Cosgrove. Analysis of Geological Structures. Cambridge University Press, Cambridge. 1990.
 - [20] Hudson, J.A, and J.P Harrison. Engineering rock mechanics: An introduction to the principles. Elsevier, Oxford, 1997.
 - [21] Elsevier Geo-Engineering Book Series Volume 4, 2006, Pages 53-97.
 - [22] B Singh 1973 CONTINUUM CHARACTERIZATION OF JOINTED. ROCK MASSES. PART II--SIGNIFICANCE OF LOW SHEAR MODULUS.
 - [23] Bray, J. (1977) Unpublished notes, Imperial College London.
 - [24] Conway, H. D. (1967). The Indentation of an Orthotropic Half Plane Having Inclined Principal Axes.

-
- [25] Sowers, G. F. (1976) Foundation bearing in weathered rock. Proc. of Specialty Conf. on Rock Eng. For Foundations and Slopes, ASCE, Geotech. Eng. Div., Boulder CO., Vol. II, pp. 32-41.
- [26] WITTKER, W.-G. f. (1984). Felsmechanik- Grundlagen für wirtschaftliches Bauen im Fels. Berlin, Heidelberg, New York.
- [27] Bowles, J. E. (1992). "Foundation Analysis and Design." McGraw-Hill.
- [28] Alexander Preh (2022) Skriptum zur Vorlesung Angewandete Felsmechanik, TU-Wien
- [29] Itasca (2023). 3 DEC (3 dimensional distinct element code) user's guide .Minneapolis, Itasca consulting group Inc.
- [30] HOEK E.2006: Practical Rock Engineering, Rock mass properties
- [31] HOEK E.1983 strength of jointed rock masses.
- [32] Paul Marinos and Evert Hoek GSI: A GEOLOGICALLY FRIENDLY TOOL FOR ROCK MASS STRENGTH ESTIMATION.
- [33] Anagnostou und Pimentel 2012 Zu den Felsklassifikationen mit Indexwerten im Tunnelbau.
- [34] Hoek E., C. Carranza-Torres 2002: HOEK-BROWN FAILURE CRITERION – 2002 EDITION.
- [35] 1 Introduction. (2006). Elsevier Geo-Engineering Book Series, 1–14.
- [36] Fecker Edwin 2018 geotechnische Messgeräte.
- [37] Strength of jointed rock masses, Evert Hoek, Golder Associates, Vancouver Canada. Twenty-third Rankine Lecture. Presented to the British Geological Society in London on February 23, 1983 and published in Geotechnique, Vol. 23, No. 3, 1983, pp. 187-223.

- [38] Numerical and Experimental Investigation on the Scaling Law of Strip Model Foundation on Cohesionless Soils Donghwi Kim a, Boo Hyun Nam b, and Heejung Youn c.
- [39] Poisel R, Preh A, Zettler A (2004) Rock as a continuous material and as a discontinuous material
- [40] Preh A (2024) Der Einfluss der Trennflächenorientierungen bei Gründungen auf Fels. Vortrag: 14. Österreichische Geotechniktagung, Wien; 01.02.2024-02.02.2024; in: 14 Österreichische Geotechniktagung ÖIAV (Hrg.); ISBN-NR. 978-3-902593-11-5; S.243-249

9 List of standards

[N.1] ONORM 81997-1-5: Eurocode 7 Entwurf, Berechnung und Bemessung in der Geotechnik, Teil 1-5 Gesamtsicherheitsnachweise von Böschungen, Hängen und Geländesprüngen Ausgabe 2017-11-0

[N.3] ONORM B1997-1-2: Eurocode 7: Entwurf, Berechnung und Bemessung in der Geotechnik Teil 2: Flächen Gründungen Berechnung der Tragfähigkeit und der Setzungen Ausgabe 2019 0701

10 List of figures

Figure .1: Characteristic values for bearing capacity from ÖNORM B1997-1-2 Figure B.1

Figure .2: Bearing capacity of a foundation on rock with inclined, approximately orthogonal joint systems (show Wyllie [11]) from ÖNORM B1997-1-2, Appendix B

Figure.3: Failure mechanisms (a) planar sliding failure on single discontinuity; (b) wedge sliding failure on two intersecting discontinuities; (c) toppling failure of steeply dipping slabs; (d) circular failure in closely fractured rock (Wyllie [11]) from ÖNORM B1997-1-2, Appendix B

Figure .4: Example of the translation of a wedge-shaped sliding body on a horizontal rock surface (show Wyllie [11]) from ÖNORM B1997-1-2, Appendix B

Figure .5: Fracture (zone A) and unfractured (zone B) on rock surface [13]

Figure .6: Mohr diagram of stresses in bearing rock [13]

Figure .7: Analysis of bearing capacity of fractured rock [13]

Figure .8: Jointed rock properties [11]

Figure .9: Numerically determined lines of equal stress ($\sigma_r = \text{const.}$) in an anisotropic, elastic and homogeneous half-space (plane distortion state. i.e. the loads are line loads) [9]

Figure .10: Load distribution in the anisotropic (transversely isotropic), elastic and homogeneous continuum [9]

Figure .11: Foundation on rock containing inclined bedding planes and orthogonal joint sets [13]

Figure .12: Spread footings on layered rock formations (a) punching failure, (b) buckling failure, and (c) bending failure. [25]

Figure .13: Mohr-Coulomb material model. [28]

Figure .14: Representation of the shear parameters in a uniaxial and triaxial stress state using stress circles [27]

Figure .15: Hoek-Brown material model [31]

Figure .16: Geological strength index for jointed rock masses [34]

Figure .17: Impact of specimen size on compressive strength [18]

Figure .18: Modification of the model properties only by changing the area under consideration [37]

Figure .19: Bearing capacity joint sets 1 according to analytical solution

Figure .20: Bearing capacity joint sets 2 according to analytical solution

Figure .21: Bearing capacity joint sets 3 according to analytical solution

Figure .22: Representation of the model for three-dimensional examinations in 3DEC

Figure .23: The appropriateness of the model dimensions under consideration of the block velocity magnitude does not extend to the boundaries.

Figure .24: The appropriateness of the model dimensions under consideration of the block displacement magnitude does not extend to the boundaries.

Figure .25: Boundary condition in numerical model

Figure .26: Model failure under Block displacement [m] with a 3 [MPa] load, with a cohesion of 0.2 [MPa] and a friction angle of 20 [°], numerical model (DEM) with 2-joint set

Figure .27: Bearing capacity for DEM model with 2joint sets and dipping $\psi_1 = 60$ [°] and $\psi_2 = 30$ [°] and Spacing 300mm

Figure .28: Wedge failure for joint sets 1 under Block displacement [m] magnitude for 2.3 [MPa] load and cohesion 0.3 [MPa], friction angel 20 [°]

Figure .29: Wedge failure for joint sets 1 under Block velocity magnitude [m/s] for 2.3 [MPa] load and cohesion 0.3 [MPa], friction angel 20 [°]

Figure .30: Wedge failure joint sets 2 under Block displacement magnitude [m] for 1 [MPa] load and cohesion 0.1 [MPa], friction angel 20 [°]

Figure .31: Wedge failure joint sets 2 under Block velocity magnitude [m/s] for 1 [MPa] load and cohesion 0.1 [MPa], friction angel 20 [°]

Figure .32: Wedge failure joint sets 3 under Block displacement magnitude [m] for 0.9 [MPa] load and cohesion 0.1 [MPa], friction angel 20 [°]

Figure .33: Wedge failure joint sets 3 under Block velocity magnitude [m/s] for 0.9 [MPa] load and cohesion 0.3 [MPa], friction angel 20 [°]

Figure .34: The impact of joint set orientation on bearing capacity in the model with 3 joint set

Figure .35: Bearing capacity through inverse calculations involving Discrete Element Method (DEM) and analytical approaches for first joint set $\psi_1 = 60$ [°] and $\psi_2 = 30$ [°]

Figure .36: Bearing capacity through inverse calculations involving Discrete Element Method (DEM) and analytical approaches for two joint set $\psi_1 = 70$ [°] and $\psi_2 = 20$ [°]

Figure .37: Bearing capacity through inverse calculations involving Discrete Element Method (DEM) and analytical approaches for third joint set $\psi_1 = 50$ [°] and $\psi_2 = 40$ [°]

Figure .38: The comparison the bearing capacity of the numerical model, which incorporates two varieties of joints, a spacing of 300 [mm], and dip direction of $\psi_1 = 60$ [°] and $\psi_2 = 30$ [°], with the analytical relationships proposed.

Figure .39: The comparison the bearing capacity of the numerical model, which incorporates three varieties of joints with friction angle 20 [°], spacing of 500 [mm], and dip direction of $\psi_1 = 60$ [°] and $\psi_2 = 30$ [°] and $\psi_3 = 90$ [°], with the analytical relationships proposed.

Figure .40: The comparison the bearing capacity of the numerical model, which incorporates three varieties of joints with friction angle 20 [°], spacing of 500 [mm], and dip direction of $\psi_1 = 70$ [°] and $\psi_2 = 20$ [°] and $\psi_3 = 90$ [°], with the analytical relationships proposed.

Figure .41: The comparison the bearing capacity of the numerical model, which incorporates three varieties of joints with friction angle 20 [°], spacing of 500mm, and dip direction of $\psi_1 = 50$ [°] and $\psi_2 = 40$ [°] and $\psi_3 = 90$ [°], with the analytical relationships proposed.

11 List of tables

Table .1: Numerical methods of analysis [10]

Table .2: Bearing capacity, Settlement intact rock [11]

Table .3: Allowable bearing pressures for fresh rocks [11]

Table .4: Approximate relationship between rock mass quality and material constant [14]

Table .5: Correction factors for foundation shapes [15]

Table .6: Classification of rock material strengths [16]

Table .7: Common elastic constants for intact rock [11]

Table .8: The orientation of the joint set in analytical solution

Table .9: Mechanical characteristics of the joint set in analytical solution

Table .10: The orientation of the joint set in DEM model with 2 joint set

Table .11: Mechanical characteristics of joint set in DEM model with 2 joint set

Table .12: The orientation of the joint set in DEM model with 3 joint set

Table .13: Mechanical characteristics of joint set in DEM model with 3 joint set

Table .14: Bearing capacity of foundation for the DEM model with 2 joint set under cohesion 0

Table .15: Bearing capacity of foundation for the DEM model with 2 joint set under cohesion 0.1 [MPa]

Table .16: Bearing capacity of foundation for the DEM model with 2 joint set under cohesion 0.2 [MPa]

Table .17: Bearing capacity of foundation for the DEM model with 2 joint set under cohesion 0.3 [MPa]

Table .18: Bearing capacity of foundation for the DEM model with 2 joint set under cohesion 0.4 [MPa]

Table .19: Bearing capacity of foundation under wedge failure for joint sets 1 with friction angel 20 [°]

Table .20: Bearing capacity of foundation under wedge failure for joint sets 2 with friction angel 20 [°]

Table .21: Bearing capacity of foundation under wedge failure for joint sets 3 with friction angel 20 [°]

Table .22: Minimum principal stress σ_{3A} through inverse calculations involving Discrete Element Method (DEM) and analytical approaches for first joint set

Table .23: Minimum principal stress σ_{3A} through inverse calculations involving Discrete Element Method (DEM) and analytical approaches for the second joint set

Table .24: Minimum principal stress σ_{3A} through inverse calculations involving Discrete Element Method (DEM) and analytical approaches for the third joint set

